ABSTRACT

Title of Document:	PROGNOSTICS OF BALL BEARINGS IN COOLING FANS
	Hyunseok Oh, Doctor of Philosophy (Ph.D.), 2012
Directed By:	Professor, Michael Pecht, Department of Mechanical Engineering

Ball bearings have been used to support rotating shafts in machines such as wind turbines, aircraft engines, and desktop computer fans. There has been extensive research in the areas of condition monitoring, diagnostics, and prognostics of ball bearings. As the identification of ball bearing defects by inspection interrupts the operation of rotating machines and can be costly, the assessment of the health of ball bearings relies on the use of condition monitoring techniques. Fault detection and life prediction methods have been developed to improve condition-based maintenance and product qualification. However, intermittent and catastrophic system failures due to bearing problems still occur resulting in loss of life and increase of maintenance and warranty costs. Inaccurate life prediction of ball bearings is of concern to industry. This research focuses on prognostics of ball bearings based on vibration and acoustic emission analysis to provide early warning of failure and predict life in advance. The failure mechanisms of ball bearings in cooling fans are identified and failure precursors associated with the defects are determined. A prognostic method based on

Bayesian Monte Carlo method and sequential probability ratio test is developed to predict time-to-failure of ball bearings in advance. A benchmark study is presented to demonstrate the application of the developed prognostic method to desktop computer fans. The prognostic method developed in this research can be extended as a general method to predict life of a component or system.

PROGNOSTICS OF BALL BEARINGS IN COOLING FANS

By

Hyunseok Oh

Dissertation submitted to the Faculty of the Graduate School of the
University of Maryland, College Park, in partial fulfillment
of the requirements for the degree of
Doctor of Philosophy
2012

Advisory Committee:
Professor Michael Pecht, Chair
Professor Steve Marcus
Professor Donald Barker
Professor Peter Sandborn
Associate Professor F. Patrick McCluskey
Assistant Research Scientist Dr. Michael H. Azarian

Dedicated to my wife (Huisuk Kang)

and parents (Joo-Chang Oh and Chae-Yeon Kim)

Acknowledgements

First of all, I would like to express my sincere gratitude to my advisor, Prof. Michael Pecht, for his invaluable guidance and suggestions. He provided me with constructive criticism and challenged me to set my goals high.

Especially, I thank Dr. Michael H. Azarian for his kind support in technical discussions and his feedback in writing papers. I also appreciate valuable comments from my PhD dissertation committee members, Prof. Steve Marcus, Prof. Donald Barker, Prof. Peter Sandborn, and Prof. F. Patrick McCluskey. Those comments helped me to improve the quality of my research.

I thank Dr. Diganta Das and Dr. Carlos Morillo for their support. I also thank Edward Rhem and Takashi Inoue for giving me a view from the industry. I appreciate help from Mark Zimmerman and Kelly Smith regarding the improvement of skills in technical writing. I gratefully acknowledge the financial support of the CALCE consortium for my research.

I am specially thankful to receive numerous comments from friends and colleagues who attended daily morning meeting at CALCE: Dr. Daeil Kwon, Dr. Sungwon Han, Dr. Jie Gu, Dr. Vasilis Sotiris, Dr. Sachin Kumar, Dr. Gilbert Haddad, Dr. Mohammed Alam, Dr. Shunfeng Cheng, Dr. Nishad Patil, Dr. Preeti Chauhan, Dr. Jun Dai, Moon-Hwan Chang, Ranjith Kumar, Jing Tian, Edwin Sutrisno, Sandeep Menon, Sony Mathew, Elviz George, Wei He, Xiaofei He, Ning Yan, Anto Peter, Fei Chai, Arvind Vasan, and Anshul Shrivastava.

Table of Contents

List of Tables vi
List of Figures vii

CHAPTER 1 Introduction 1
1.1 Bearings 2
1.2 Bearing Health Monitoring 3
1.3 Motivation 4
1.4 Organization 5

CHAPTER 2 Literature Review 7
2.1 Condition Monitoring for Rolling Element Bearings 7
2.2 Fault Detection for Rolling Element Bearings 9
2.2.1 Analytical Approach 10
2.2.2 Artificial Intelligence Approach 12
2.3 Bearing Life Prediction 13
2.3.1 Physics-of-Failure Approach 14
2.3.2 Data-Driven Approach 14
2.4 Summary of Literature Review 17
2.5 Problem Statement 18

CHAPTER 3 Research Approach 19
3.1 Bearing Samples 20
3.2 Experimental Setup 21
3.2.1 Equipment for Bearing Testing 21
3.2.2 Hardware and Software for Vibration and AE Measurement 22
3.3 Feature Extraction 23
3.3.1 Features from Vibration Signal 24
3.3.2 Features from AE Signal 24

CHAPTER 4 Functional Relationship between Vibration (or Acoustic Emission) and Bearing Defects 32
4.1 Failure Analysis 33
4.1.1 Surface Characterization 34
4.1.2 Infrared Spectra Analysis 36
4.1.3 Surface Topology Analysis 37
4.2 Correlation Analysis 39
4.3 Sensitivity of Vibration and AE Features to Fault Detection 40
4.4 Summary 41

CHAPTER 5 Bearing Life Prediction Based on Bayesian Monte Carlo Method and Sequential Probability Ratio Test 61
5.1 Trending the Evolution of Health Monitoring Index 61
5.2 Parameter Estimation Using Bayesian Monte Carlo Method 63

5.3 Probability Distribution Estimation Using SPRT 66
5.4 Bearing Life Prediction 68
5.5 Life Prediction of Ball Bearings in Fans 69
5.5.1 Parameter Initialization in the Life Prediction Model 70
5.5.2 Results 70
5.6 Summary 71

CHAPTER 6 Contributions and Future Work 76

Appendix 78
A. Determination of Failure Criterion 78
References 81

List of Tables

Table 1 Definition of AE Hit-Driven Feature 26
Table 2 Definition of AE Time-Driven Feature 27
Table 3 Concentration of Debris Taken from Bearing with Grease after Failure 43
Table 4 Equation Used for Terms Removal 43
Table 5 Definition, Calculation, and Use of Surface Measurement Parameters [68]. 43
Table 6 Surface Roughness of Balls in Bearings: Roughness Average (R_a) 44
Table 7 Surface Roughness of Balls in Bearings: Maximum Height (R_t) 44
Table 8 Summary of Failure Analysis Results 45
Table 9 Comparison of Fault Detection Times of Vibration and AE Features 46
Table 10 Comparison of Fault Detection Times of Vibration and AE Features 46
Table 11 Rank of Vibration Features in Terms of Correlation Coefficient between Feature and Surface Roughness (R_t) 46
Table 12 Rank of AE Features in Terms of Correlation Coefficient between Feature and Surface Roughness (R_t) 47
Table 13 Predicted Failure Time and Actual Failure Time 73
Table 14 Prediction Error 73
Table 15 Failure Criteria of Fans in IPC-9591 [76] 80

List of Figures

Figure 1 Categorization of Bearings 6
Figure 2 Ball Bearing Elements: Balls, Inner and Outer Races, and Cage 6
Figure 3 Ball Bearing Used in Tests 28
Figure 4 Fan Sample (93 mm × 93 mm × 38 mm) 28
Figure 5 Duty Cycle in Pulse Width Modulation (PWM) Signal 28
Figure 6 Test Fixture: A Fan is mounted on the test fixture 29
Figure 7 Fan Mounted on Test Fixture with Accelerometer and AE Transducer 29
Figure 8 System for Vibration and Acoustic Emission Monitoring 29
Figure 9 Identification of One Hit by Specified Hit Definition Time 30
Figure 10 AE HD Feature: Peak Amplitude, Hit Duration, Rise Time, and Hit Count 30
Figure 11 HD Absolute Energy 31
Figure 12 TD Absolute Power 31
Figure 13 Experimental Procedures 48
Figure 14 Evolution of Vibration of Ball Bearings with Oil 48
Figure 15 Evolution of AE of Ball Bearing with Oil 49
Figure 16 Naming Bearing A and B in a Fan 49
Figure 17 Bearing with Oil (Failure): debris indicated by arrows was found 50
Figure 18 Bearing with Oil (Unused): no debris was found 51
Figure 19 Bearing with Oil (Partially Degraded): debris indicated by arrows was found 51
Figure 20 Bearing with Oil (Partially Degraded): debris indicated by arrows was found 52
Figure 21 Bearing with Grease (Failed): debris indicated by arrows was found 53
Figure 22 Spots Used for Chemical Concentration Analysis 54
Figure 23 Comparison of Infrared Spectra Using Oil from Unused, Partially Degraded, and Failed Ball Bearings 55
Figure 24 Comparison of Infrared Spectra Using Grease from Unused and Failed Ball Bearings 55
Figure 25 Surface Topology of Ball from Bearing with Oil that Partially Degraded. 56
Figure 26 Surface Topology of Ball from Bearing with Oil that Failed 56
Figure 27 Surface Topology of Ball from Bearing with Oil that Operated after Failure 57
Figure 28 Surface Topology of Ball from Bearing with Grease that Failed 57
Figure 29 AE Hit-driven Rise Time of Ball Bearings with Oil (failed at 66.2 hours) 58
Figure 30 AE Hit-driven Hit Duration of Ball Bearings with Oil (failed at 66.2 hours) 58
Figure 31 AE Hit-driven Hit Count of Ball Bearings with Oil (failed at 66.2 hours) 59
Figure 32 Correlation between Vibration Peak and Surface Roughness (R_t) 59
Figure 33 Correlation between AE Hit Count and Surface Roughness (R_t) 60
Figure 34 Vibration rms from Stress Tests of Bearings (Black Line) and Smoothened Vibration rms (Red Dots) 74

Figure 35 Smoothened Vibration rms (Red Dots) and Fitting of the Vibration rms Using Compound Model (Blue Lines)..... 74
Figure 36 Flowchart to Adapt Probability Distribution Using SPRT..... 75
Figure 37 Ball Bearing Used in Tests..... 80

CHAPTER 1 Introduction

Bearing failure can result in catastrophic and/or intermittent failure of the system. System failures due to bearing problems resulted in loss of life and increase of maintenance and warranty costs. For example, the crash of a Navy CH-53 helicopter resulted in the loss of 4 people and replacement cost of 30 million to the helicopter manufacturer, Sikorsky [1]. The bearing manufacturer paid 7.5 million in fines to US government. The accident triggered the grounding of the entire H-53 fleet in US for three months. Another example is the failure of cooling fans in electronic systems. IBM identified that bearings were the most critical component for determining cooling fan reliability [2]. According to Pareto analysis by HP [3], mechanical failures of cooling fans were 43% of all the failures observed in the field and bearing failure was the top contributor to the mechanical failure, resulting in the increase of warranty and maintenance costs. In [4], it was reported that bearing failures are responsible for 40% ~ 50% of all failures of induction motors.

There is growing interest in prognostics and health management (PHM) of a component or system. PHM is an enabling discipline consisting of technologies and methods to assess the reliability of a product in its actual life cycle conditions to determine the advent of failure and mitigate system risk [5]. Bearing PHM is a potential way to improve qualification and screening of rotating devices, enable condition-based maintenance of products in the field, and enhance the design of future products.

PHM methodologies have following aspects: health monitoring, fault detection, life prediction, and decision making. Health (or condition) monitoring is

the process of acquiring sensor data from the operating component or system. Health monitoring provides information regarding the operational status and performance of the component or system. For bearing health monitoring, sensor data includes vibration, acoustic emission, shock pulse, motor current, wear debris, and temperature. A database of sensor data is the fundamental information used to estimate the evolution of bearing degradation, detect faults and predict remaining life for bearings.

This chapter starts with the description of bearings and health monitoring techniques. Then, motivation and organization of this thesis are presented.

1.1 Bearings

Bearings are used to support the rotating shaft in rotating devices or machines. Figure 1 shows the categorization of bearings. There are two types of bearings depending on the relative motion between bearing elements: sliding bearings and rolling element bearings. Rolling element bearing is further divided into roller and ball bearings. Ball bearing elements include balls, inner and outer rings, and a cage. Figure 2 illustrates the construction of ball bearings. The cage is used to locate balls in the designed position. Oil, grease, or solid film is used for the lubrication of the bearing elements. Ball bearings can have shields or seals on both sides to protect against dirt or contaminants. This research focused on ball bearings sealed with lubricant. This type of ball bearings is widely used in rotating devices in electronics.

The life of ball bearing is described by using Weibull distribution, since the life of bearing is not deterministic. The fatigue life of a population of bearings is described in terms of L_{10} life (number of revolutions to failure of 10% of the population). L_{10} life is a function of loads applied to bearings. Equations for

calculating L_{10} bearing life is available in catalogs from bearing manufacturers. The effect of bearing lubricant deterioration, contamination by external dirt or dust, and the increase of operating temperature on L_{10} bearing life can be accounted for by the use of modification factors. The ISO 281 standard [6] provides bearing life equations that incorporate modification factors such as lubrication, environment, contaminant particles, and mounting.

1.2 Bearing Health Monitoring

Health monitoring is to collect sensor information from a component or a system of interest. Techniques for health monitoring include vibration, acoustic emission, shock pulse, motor current, wear debris, and temperature analysis. The type of health monitoring techniques can be selected depending on applications.

Vibration analysis has been used to detect defects of bearings [7][8]. A surface with damages in the form of distributed or localized defects is a source for the increase of mechanical vibration. When distributed defects arise, the variation of contact force between balls and other elements results in an increased level of vibration. When localized defects exist, a sudden change of contact force at the interface generates a pulse within a short period of time. The pulse produces vibration that indicates the existence of defects in the ball bearing. Therefore, vibration analysis has been a widely used to monitor the health of bearings.

Acoustic emission (AE) is defined as the generation of elastic waves released from localized sources within a material when the material undergoes deformation [9]. Acoustic emission is different from vibration in terms of generation of the signal. Vibration occurs when a ball passes over defective surfaces of other elements. If a

defect does not exist, an increased level of vibration will not be observed. AE occurs due to the deformation of materials. The wearout of bearing surfaces is often associated with the deformation of bearing materials, thus generates AE waves. Examples of physical processes that generate AE include plastic deformation (or fracture) of asperities on the surface of bearing elements, contaminant and/or wear particles. Therefore, acoustic emission analysis is a relevant health monitoring technique to detect bearing defects.

1.3 Motivation

Despite the advance of technologies to detect bearing faults and predict bearing life, intermittent and catastrophic system failures due to bearing problems still occur. Accidents and incidents such as Navy MH-53E helicopter crash [10], emergency landing of Airbus 330 [11], pump failure [12], and computer cooling fan failure [13] resulted in loss of life and increase of maintenance and warranty costs. Therefore, issues related to fault detection and life prediction of ball bearings needs to be investigated.

The reliability of ball bearings can be described in the form of L_{10}. L_{10} life is useful to describe the life of a population of bearings due to failure by material fatigue. However, it is common to observe a different failure time for identical ball bearings operating under the same loading condition. For example, the lifetime of identical bearings operating under the same testing condition varied more than seven times [14][15]. As we have seen in the examples of system failure, fault detection and life prediction for a particular bearing of interest are sometimes more valuable to prevent accidents and incidents by bearing failure.

1.4 Organization

The remainder of this document is organized as follows. Chapter 2 provides the literature review on fault detection and life prediction of ball bearings. Fault detection based on sequential probability ratio is discussed. The gaps in the literature are presented. Chapter 3 describes the research approach used in this research. The experimental setup and feature extraction from health monitoring signals are presented. Chapter 4 describes the correlation between features and results from failure analysis. Potential features for bearing fault detection and life prediction are discussed. Chapter 5 presents the development of a prognostic model based on Bayesian Monte Carlo method and sequential probability ratio test. Chapter 6 describes the contributions and future work.

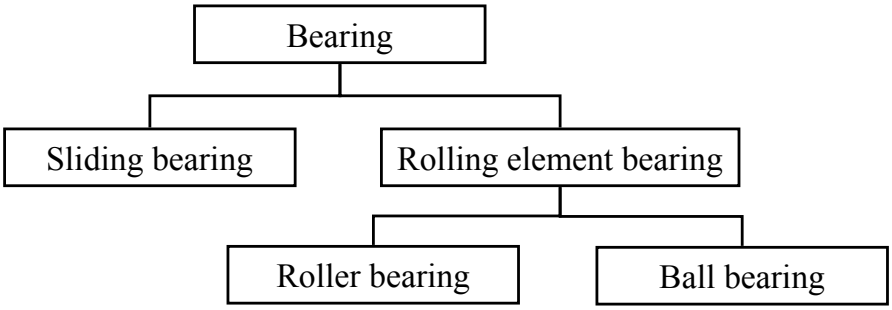

Figure 1 Categorization of Bearings

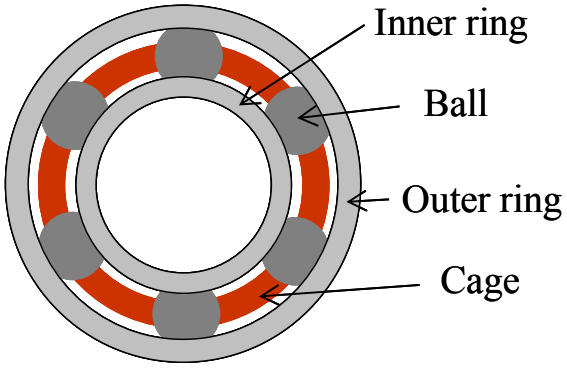

Figure 2 Ball Bearing Elements: Balls, Inner and Outer Races, and Cage

CHAPTER 2 Literature Review

The literature review includes the following aspects: 1) condition monitoring for rolling bearings; 2) fault detection for rolling bearings; 3) bearing life prediction; The literature review is followed by the problem statement.

2.1 Condition Monitoring for Rolling Element Bearings

Condition monitoring is to acquire sensor data from bearings in a rotating machine. Sensor data used for condition monitoring of rolling element bearings comes from the measurements of vibration [15]-[20], acoustic emission [15]-[19][21][22], acoustic sound [23], and shock pulse [18][19], oil/wear debris [20][28] and temperature [20]. For ball bearings placed in electrical motors, electrical current is used to monitor the health of ball bearings [18][19][24].

AE hit count rate was correlated with dry contacts of bearing steels [25][26] and rolling contact fatigue of steel alloy [27]. AE count rate was proportional to the surface damage of the material.

Williams et al. [15] monitored the evolution of vibration and acoustic emission from fatigue life testing of rolling element bearings. The authors claimed that their research is the first one to monitor the evolution of vibration and acoustic emission due to material fatigue, while the previous research focused on the detection of artificially seeded defects. The experimental results showed that vibration and acoustic emission do not always increase during the life testing, but showed transient behavior. The observation was different from those from tests using bearings with

artificially seeded defects, which showed a linear relationship between vibration and defect size.

Al-Ghamd and Mba [17] compared the sensitivity of vibration and acoustic emission signals to detection of defects artificially seeded to roller bearings. The authors reported that AE in terms of rms, peak amplitude, and kurtosis showed higher sensitivity than vibration signals to early detection of bearing defects. A linear relationship between AE hit duration and defect size was identified.

Tandon et al. [18] investigated the sensitivity of vibration, acoustic emission, shock pulse, and electrical current to detection of bearing defects in induction motors. Defects in the form of a circular hole with the diameter from 0.25 mm to 1.5 mm were artificially seeded to bearings. Measurements were conducted with a constant speed and load from zero to the dynamic load rating of the bearing. AE showed the best performance in terms of bearing fault detection followed by electrical current. Another research by Tandon et al. [19] investigated the effect of contaminants in bearing grease to vibration, acoustic emission, shock pulse, and electrical current. Grease mixed with silica and ferric oxide particles were intentionally injected into ball bearings. AE in terms of peak amplitude showed the best sensitivity in terms of percentage increase of the signals among other condition monitoring techniques for ball bearings.

Craig et al. [20] investigated the correlation between wear debris in bearing oil and other condition monitoring techniques including vibration and temperature analysis. A cone-shape indent with the diameter of 400 μm was seeded to induce fatigue crack on the surface of bearing elements during life testing. The study showed

that the transition from the healthy condition to failure occurred when wear debris detected was within the range of 5 μm to 15 μm. At the time of the transition, other condition monitoring technique was insensitive to the transition.

Even though vibration is the most widely used condition monitoring technique, acoustic emission showed early detection of bearing defects than other condition monitoring technique except wear/oil debris analysis. The use of wear/oil debris analysis technique requires is limited. When the amount of oil or grease in bearings is too small to be sampled, the sampling will interrupt lubricant between bearing elements.

The effectiveness of condition monitoring technique to bearing defect detection was evaluated by using bearing with artificially seeded defects rather than using bearings from life testing. AE features including hit count rate, hit duration, peak amplitude, rms, and kurtosis were sensitive to early detection of bearing faults. The functional relationship between AE hit counts and wear volume (or frictional work) in sliding friction of metals was modeled by Lingard and Ng [29].

2.2 Fault Detection for Rolling Element Bearings

Bearings degrade by mechanisms such as fatigue, corrosion, contamination, wear, and lubricant deterioration [4][30][31]. When repetitive mechanical stress between the fatigue limit and the ultimate strength of the material are applied to bearings, the bearings can fail due to material fatigue. Cracks are initiated below the surfaces of bearing elements by cyclic loading and propagate towards the surfaces, resulting in spalls. A spall is a defect where metallic particles are flaked off from the surface.

Deterioration of grease in permanently lubricated ball bearings is caused by thermal overloads. Lubrication deterioration due to thermal overloads can be in the form of either physical or chemical degradation [32]. The physical degradation is due to lubricant evaporation. The chemical degradation is caused either by antioxidant consumption or lubricant oxidation. Lubricant deterioration leads to poor lubrication between bearing elements, resulting in seizure, the state of stopping relative motion between bearing components as a result of interfacial friction.

To detect ball bearing faults, two approaches have been used: analytical and artificial intelligence (AI) approaches in bearing PHM. Analytical approaches utilize signal processing techniques to improve signal-to-noise ratio of extracted features to detect defects in bearings. A fixed threshold level may be used to classify the conditions of bearings in analytical approach. AI approach classifies the severity of defects in bearings based on machine learning techniques such as neural networks [33][34], support vector machines [35]-[38], relevance vector machine [39], k-nearest neighborhood [40], hidden Markov models [41], and decision tree [42]. Details of the two approaches are described in the following subsection.

2.2.1 Analytical Approach

Vibration signals are processed in either the time or frequency domains. Time domain features include root mean square (rms), peak amplitude, crest factor (peak amplitude divided by rms), and kurtosis. Frequency domain features are bearing defect frequencies and its harmonics. Bearing defect frequencies are characteristic frequencies associated with bearing elements. When balls in a bearing pass over defects on the surface of the inner and outer races, mechanical pulses are generated.

The repetitive impacts produce vibration signals during the running of the bearing. Bearing defect frequencies for rolling elements and inner and outer races can be calculated based on the geometry and rotating speed of a bearing [7].

Envelope detection technique (or high frequency resonance technique) is useful to increase signal-to-noise ratio for fault detection of bearings [43]-[45]. When bearing elements generate repetitive impacts due to defects, the repetitive impacts not only generate distinct bearing defect frequencies, they also excite the resonance frequencies of the machine structure that supports the bearing itself. Envelope detection technique extracts information associated with bearing defects in the resonance frequency.

Shiroishi et al. [46] investigated the performance of a signal processing method that combined high-frequency resonance technique with adaptive line enhancer. Defects in the form of cup or cone scratches were artificially seeded in the bearings. Vibration peak was the most sensitive to the defects followed by vibration processed by the signal processing method, vibration rms, kurtosis, and crest factor. AE was insensitive to the cone defects on the inner race of bearings. A linear relationship between vibration peak and defect size at the bearing rotational speed of 1200 rpm was identified with the correlation coefficient of 0.971.

Another signal processing technique for de-noising and extracting weak signal is wavelet filtering. Qiu et al. [47] compared two methods including wavelet transform based de-noising and wavelet filtering based de-noising. Vibration from a bearing with artificially seeded faults was used for the comparison. The wavelet filter was showed better sensitivity to detect a weak signature of “mechanical impulse-like”

detect signals while the wavelet transform method performed better to detect "smooth" signals. The study investigated the sensitivity of signal processing technique. However, the determination of the sensitivity was qualitative.

Increase of "generalized roughness," which is spatially distributed roughness on a bearing surface, is a defect which commonly occurs in rolling bearings. Frequency domain analysis sometimes fail to detect increased generalized roughness due to broadening of spectral peaks associated with bearing defects, even though signal processing techniques such as envelope detection or wavelet filtering techniques are applied. To detect generalized roughness faults of bearings, Immovilli et al. [48] demonstrated that a time-frequency index, spectral kurtosis, was effective.

2.2.2 Artificial Intelligence Approach

Boutros and Liang [41] developed fault detection and diagnosis methods based on HMMs. Defects with the diameter of 0.007", 0.014", and 0.021" were seeded on the surface of bearing elements by electro-discharging machining. The method achieved 95% of classification accuracy to detect faults seeded in bearings. The time required for training the HMMs was less than 5 seconds.

Zarei [33] proposed a fault diagnosis method based on ANNs and time domain features from vibration analysis. The method classified three types of scenarios of bearing conditions including healthy, faulty inner race, and fault outer race. The developed method classified the faults with the accuracy more than 96%.

Gryllias and Antoniadis [35] developed an SVM approach to classify defects in rolling element bearings in industrial environments. In the approach, two steps were used: training of SVM using simulation data and testing the trained SVM using

data obtained from the field. The trained SVM showed 100% classification accuracy for 34 vibration measurements collected from bearings with faulty inner races and faulty outer races.

Yiakopoulos et al. [40] developed a K-means clustering approach to provide an automated way for bearing fault detection. The same dataset in [91] was used to evaluate the performance of the proposed method. The approach achieved 100% classification accuracy.

Sugumaran et al. [37] developed a decision tree approach to identify faulty elements in bearings of interest. The decision tree based method was tested using vibration features collected from healthy bearings, faulty bearings with inner race defect, faulty bearings with outer race defect, and faulty bearings with both inner and outer race defects. The results showed that misclassification rate was less than 5%.

The AI-based approaches attempted to provide automatic ways to detect bearing faults and diagnose faulty bearings. The benefit for using the AI based approach is that the number of human interventions is minimized. AI algorithms determine if a particular bearing of interest is healthy or faulty.

2.3 Bearing Life Prediction

Bearing prognostics includes two approaches: physics-of-failure (PoF) and data-driven (DD). PoF-based methods use knowledge of material properties, product geometry, life cycle loading, and PoF models to estimate the life of a product. DD-based methods do not require specific knowledge of a product such as material properties, structure geometry, and failure mechanism. DD-based methods extract information from historical data of the performance of a product to capture trends of

product health and predict the life using machine learning techniques, and statistics and probability theory [49].

2.3.1 Physics-of-Failure Approach

Crack growth models based on Paris' law are typically used for predicting the crack length in the future [50]-[52]. Li et al. [50] addressed the stochastic characteristics of crack propagation. In order to reflect the stochastic nature into the PoF model, the authors added a random variable with lognormal distribution to the deterministic defect-propagation rate model (i.e., Paris' law). The random variable considers uncertainties and inaccuracies with the deterministic model, and errors associated with estimating parameters. The prognostic algorithm estimates the mean and variance of the defect propagation path. The authors reported that, before 10% of the bearing life, the proposed method was able to predict the remaining useful life of the bearing with the accuracy of ±2.5%. This high accuracy is possible since the model reflect the nature of bearing degradation and the test was conducted under controlled laboratory conditions.

Kacprzynski, et al. [53] presented a framework for predicting remaining life by PoF models with diagnostic capabilities. For the prediction, several PoF models are used including the stress-strain model for calculating energy required for crack initiation, Paris' crack growth model for calculating crack propagation.

2.3.2 Data-Driven Approach

Trend projection is a simple way to make predictions. The assumption of trend projection is that the future states will follow the degradation pattern of the past. Cempel [54] proposed a tribo-vibroacoustical (TVA) model for predicting the time-

to-failure by estimating the vibration amplitude. Life predictions can result in big errors if trending algorithms are not stable during bearing degradation. However, the method is effective when the computational power is limited, since trend projection does not require lots of calculation.

Time series prediction methods are useful to forecast future conditions within a short time over the bearing life. Shao and Nezu [55] developed an ANN-based time series prediction model for forecasting future condition of bearings in terms of vibration, although this does not provide a life prediction. Another type of ANN, recurrent neural network (RNN), was used to make multistep ahead predictions for nonlinear and non-stationary time series. An RNN has closed feedback loops in the networks. The RNN stores the previous time series values in the network and offers a value one step ahead. The RNN-based prognostic methods showed better performance compared to methods including ARMA models, bilinear models, and feed-forward type ANNs [56][57]. Pham and Yang [58] proposed a hybrid model by combining the ARMA and generalized autoregressive conditional heteroscedasticity (GARCH) models. The GARCH model aims to reflect a nonlinear trend during the bearing degradation. The authors could achieve improvements for predicting bearing life up to 5 steps of the vibration signal sampling steps, which corresponds to approximately less than 1% of the bearing life. Although, the hybrid model of the ARMA and GARCH models may capture the nonlinear characteristics of bearing degradation, the prognostic distance such 1% of the bearing life is too short to make logistic decisions for further actions.

Weight application prediction method provided life predictions of bearing with high accuracy. Gebraeel et al. [59] developed a weight application prediction method with ANN regression model. Individual ANN regression model of the prediction method was trained using a set of historical data of one bearing. The result showed that 92% of the predictions of bearing life were within 20% of actual bearing life. Huang et al. [60] developed a method to improve Gebraeel's work focusing on life prediction of ball bearings at early stage of degradation. Huang et al. used 10 samples to train each self-organizing map (SOM) regression model. Huang et al. reported that 85% of the predictions were within 20% of actual bearing life. Weight application prediction methods provided small prediction errors for bearing life. However, collecting historical data on identical bearings that covers possible degradation scenarios and training each regression model using the historical data can be time consuming and expensive.

Particle filtering (or sequential Monte Carlo methods) estimates the state of a nonlinear system with non-Gaussian noise. When the response of a system is linear with Gaussian noise, Kalman filter provides the optimal solution. When the response of a system is nonlinear, extended Kalman filter provides an approximation of the optimal solution by linearizing the non-linear response. When the response of a system is nonlinear and noise is non-Gaussian, analytical solution does not exist. By using a numerical method based on simulation (i.e., particle filtering), an approximation of the solution can be obtained. Orchard and Vachesevanos [61] presented a particle filter-based framework to estimate the length of cracks in a gear plate and predict the probability distribution of failure times. In order to overcome the

assumption of the state space model that a system's current state is dependent only on the previous state, Chen et al. [62] proposed a particle filtering method combined with adaptive neuro-fuzzy inference system (ANFIS). The process equation in the state space model was integrated with a trained ANFIS and the current state of the process equation was estimated using particle filtering.

Saha and Goebel [63] proposed a normal random walk method that changed model parameters of a process equation in the state space model. Sun et al. [64] presented the application of state space modeling technique to system prognostics. In their work, the model parameters in the linear process equation were updated based on sufficient statistics. Gabraeel et al. [13] developed a Bayesian method to predict residual life distributions of a component by using real-time condition monitoring information of the component. Model parameters in an exponential equation for the degradation were updated, as new information from sensors became available. Gabraeel pointed out that the accuracy of the predicted result of life distribution was poor when the independent and identically distributed (iid) error term was used in the process equation, since the iid error did not account for the stochastic nature of the bearing degradation due to material fatigue under mechanical loading. Zhou et al. [65] extended Gebraeel's study to the cases when the time interval between sensor measurements is not fixed.

2.4 Summary of Literature Review

Research on fault detection of ball bearings focused on the detection of artificially seeded defects. Analytical approaches such as signal processing techniques helped to increase signal-to-noise ratio of features extracted from sensor

measurements. AI approaches helped to determine if a particular bearing of interest has defects (i.e., fault classification). The evolution of bearing defects and condition monitoring information from a defect-free condition to failure of bearings was investigated from life testing of bearings that fail due to material fatigue.

PoF approaches demonstrated that life prediction accuracy can be within 2.5% for bearings that failed due to fatigue. DD approaches have been developed to make life prediction of bearings based on techniques such as autoregressive moving averaging, neural networks, weight application, relevance vector machines, and particle filtering. ARMA-based prognostic methods forecasted future conditions of bearings, although this does not provide a life prediction. WA based methods demonstrated that prediction errors were within 20% of actual life of bearings that fail due to material fatigue.

2.5 Problem Statement

- The evolution of defects and health monitoring indices for bearings operated under thermal and mechanical loading below the fatigue load limit was not identified.
- A life prediction method was not developed for bearings operated under thermal and mechanical loading below the fatigue load limit.

CHAPTER 3 Research Approach

Condition monitoring techniques including vibration and AE analysis will be used to quantify the health of bearings and predict life of bearings. There were lots of applications regarding the use of condition monitoring techniques to measure the degradation of bearings in rotating machines such as aircraft engines and wind turbines. However, little attention has been paid to applications of the condition monitoring techniques to lot acceptance or screening out defective fans in the electronics industry. There were issues that should be accounted for when the vibration- or acoustic emission-based techniques are applied to estimate the condition of fans. For example, the weight of an accelerometer should be less than 5% of the total weight of a fan. Otherwise, vibration measurement results from an accelerometer will not be correct due to the loading effect. A test fixture where fans are mounted should be able to isolate vibration from external sources. Therefore, a key step is to design and build an experimental setup capable of measuring the degradation of fan bearings expected in electronics industry.

The bearing degradation in a fan may take up to 3 to 5 years depending on operational loading conditions. Completing life tests within a reasonable amount of time duration is a challenge. Two separate life tests will be conducted simultaneously: in situ monitoring stress test and long-term stress test. The objective of in situ monitoring stress test is to monitor the degradation of bearings in a particular fan of interest. Data from vibration and AE sensors are continuously collected in order to monitor the degradation of fan bearings closely. The purpose of long-term stress tests

is to capture degradation of bearings in multiple fans. Due to the limitation of the resources to collect data from bearings in multiple fans, the sensor signals of the fans will not be measured continuously but periodically. From both of the in situ monitoring and long-term stress tests, we will be able to build a database of vibration and acoustic emission signals for further analysis.

3.1 Bearing Samples

Ball bearings from NSK Ltd., part number 693ZZ, are used in the test. The inner and outer diameters of the bearing are 3 mm and 8 mm, respectively. As shown in Figure 3, a bearing is composed of balls, a cage, and inner and outer races. The balls and inner and outer races are made of stainless steel (SUJ 2). The cage is made of reinforced polyamide plastic. The cage is composed of 10% weight of glass fiber and 90% weight of polyamide 66.

The bearing contains both oil (Winsor Lube L245X, maximum operating temperature: 300°C) and grease (NS7, maximum operating temperature: 130°C) for lubrication between bearing elements. The oil and grease are intentionally added to the bearings during the manufacturing process of bearings. The sequence of the manufacturing process is described as follow. After bearing elements are fabricated and assembled, the bearing assembly is cleaned and soaked in the oil for internal lubrication. The bearing assembly is taken from the oil bath and the residual oil is drained off. A particular amount of grease is added into the bearing assembly. Then shield plates are mounted to the both sides of the bearing assembly. A normal bearing contains 11 milligrams of grease. Bearings with oil but no grease and bearings with both oil and 3 milligrams of grease were used.

3.2 Experimental Setup

The operation of bearings was conducted using fan assemblies with the bearings. Bearings are located in fans to support the rotating shaft of the fans. Fans used in the test are Nidec M35556-35DEL shown in Figure 4. The rated voltage and current are 12VDC and 1.0A, respectively. The rated speed is 4,800 rpm. The range of the operating temperature of the fan is -10°C to 70°C.

3.2.1 Equipment for Bearing Testing

We used a power supply (Agilent N5744A: voltage range of 0 to 20V, current range of 0 to 38A, max power of 750W) to supply electrical power to the fan (rated voltage of 12VDC, rated current of 1.0A). The rotational speed of the fan can be controlled by changing the duty cycle of the PWM signal that is another input to the fan. The definition of the duty cycle is shown in Figure 5. A signal generator (Agilent 33120A) was used to provide a PWM signal to the fan. The duty cycle of the pulse that the signal generator can generate is limited between 20% and 80%. When the fan is required to rotate the full speed, we generated a PWM signal with a 100% duty cycle by using a power supply (Agilent E3630A). The PWM signal with a 100% duty cycle is a constant voltage of +3VDC from the power supply.

By using the power supplies and signal generator, we were able to control the speed of the fan: 1440 rpm (0% duty cycle), 2112 rpm to 4128 rpm (20% to 80% duty cycle), and 4,800 rpm (100% duty cycle). The allowable variation of the fan speed was ±10% of the normal speed of the fan.

Two ovens were used for stress tests of fans under elevated temperature conditions. Long term stress tests were performed using a BMA TC-4 oven. The

temperature in the BMA TC-4 oven can be controlled between room temperature and +220°C. In situ tests were performed using a Yamato DVS 612CE oven. The temperature in the Yamato DVS 612CE can be controlled between +5°C and +260°C, when no heat source is located in the oven. The temperature in the oven can be controlled between +70°C and +260°C, when a heat source of 300W is located in the oven.

A test fixture was fabricated in accordance with ISO 10302-2 [66] to measure the vibration of a fan at room temperature. For in situ monitoring test of a fan, another test fixture was fabricated enough to be fitted into the oven as shown in Figure 6.

3.2.2 Hardware and Software for Vibration and AE Measurement

A model 352A24 accelerometer from PCB Piezotronics Inc. was used to measure vibration of bearings in a fan. The accelerometer has a weight of 0.8 grams and a frequency range of 0.8 Hz to 10 kHz with ±10% linearity. A model PCI-4474 data acquisition (DAQ) board from National Instruments (NI) was used to digitize the vibration signal from the accelerometer. The condition monitoring system is illustrated in Figure 8, where the PCI-4474 board is labeled “data acquisition board #1. The operation of the accelerometer and PCI-4474 board was controlled by using NI LabVIEW version 8.5.1 software. By using the vibration monitoring system, including the accelerometer, DAQ board, and software, vibration signals from bearings in a fan were collected and processed.

A model Nano 30 acoustic emission transducer from Physical Acoustics Corporation (PAC) was used to measure acoustic emission from bearings in a fan, as shown in Figure 7. The acoustic emission transducer has a weight of 0.5 grams and an

operating frequency band of 125 kHz to 750 kHz. The signal from the acoustic emission transducer passed thorough PAC 2/4/6 amplifier with the amplification of 40 dB. For the collection of acoustic emission signals, another DAQ board, PAC PCI-2, is used. This setup is illustrated in Figure 8, where the PAC PCI-2 board is labeled "data acquisition board #2". The operation of the AE transducer and PAC PCI-2 DAQ board was controlled by PAC AEwin version 3.6.1 software. By using the acoustic emission monitoring system, including the AE transducer, amplifier, DAQ board, and software, AE signals from bearings in a fan were collected and processed.

The accelerometer and AE transducer were mounted to the fan surface in a manner that allowed repeated mounting and removal of the sensors. Petro wax, which was obtained from PCB Piezotronics, was used at room temperature for this purpose. However, at temperatures above room temperature Petro wax cannot be expected to provide good bond strength. Loctite 4501 adhesive guarantees the bond strength up to 100°C for 2,000 hours. Another adhesive, Loctite 4212, guarantees the bond strength up to 121°C for 1,500 hours. For in situ tests operating above room temperature, the use of one of these Loctite adhesives was necessary to ensure stable attachment of the sensors for good measurement quality. When either of the Loctite adhesives is used, the sensors can be removed from the surface with the use of acetone.

3.3 Feature Extraction

The performance of fault detection and life prediction methods depends on the sensitivity of features used to estimate the severity of bearing defects. Several features can be extracted from vibration and AE signals. The features used in this thesis are described in the following sections.

3.3.1 Features from Vibration Signal

Vibration signals are processed in time domain: rms: peak amplitude, kurtosis, crest factor, and amplitude at 99.9%. Amplitude at 99.9% was developed and used, since rms is not sensitive to sudden change of vibration and peak amplitude is susceptible to noise from external sources. Procedures for calculating amplitude at 99.9% are as follows: 1) prepare time series of vibration signals; 2) calculate absolute values of each data point in the time series; 3) arrange the absolute values from the lowest to the highest; 4) select the absolute value corresponds to the percentage rank of 99.9% from the arrangement.

3.3.2 Features from AE Signal

There are two types of AE features: hit-driven (HD) and time-driven (TD) features. HD features focus on the characteristics of a single AE event. A single AE event is defined as multiple AE hits whose waveform signal exceeds a predetermined threshold. An HD feature is only recorded if the threshold is exceeded. The threshold is commonly expressed in the unit of dB with a reference of 1μVolt. On the other hand, TD features focus on the characteristics of an AE waveform over the entire AE duration. TD features are detected regardless of the threshold level.

Before defining HD features, it is valuable to clarify "AE hit." A term, hit definition time (HDT), is used to define the start of an AE hit and the end of the AE hit as shown in Figure 9. A setting of the HDT requires so that a single occurrence of AE is reported as one and only one hit. The setting of all the three terms should be based on the characteristics of a material that generates acoustic emission. For metal

specimens, the HDT value recommended by Physical Acoustics Corporation is 600 μsec.

HD features focus on the characteristics of a single AE event. A single AE event is defined as multiple AE hits whose waveform signal exceeds a predetermined threshold. Twelve HD features are discussed: peak amplitude, rise time, hit duration, count, absolute energy, PAC energy, signal strength, root mean square, average signal level, peak frequency, average frequency, and frequency centroid. TD features focus on the characteristics of an AE waveform over the entire AE duration. TD features are detected regardless of the threshold level. Three HD features are discussed: root mean square, absolute power, and average signal level. An illustration of the definition of AE features including peak amplitude, hit duration, rise time, hit count, absolute energy, and absolute power are shown in Figure 10, Figure 11, and Figure 12.

Table 1 Definition of AE Hit-Driven Feature

AE feature	Definition	Illustration
Rise time	Rise time is defined as the time between the first threshold-crossing and the peak of the hit.	Figure 10
Peak amplitude	Peak amplitude is the maximum amplitude of an AE waveform. The peak amplitude could be taken from negative or positive maximum voltage of an AE waveform although positive peak amplitude is shown in the illustration. Peak amplitude (dB) = 20 log ($V_{max}/(10^{-6})$) - G_{pre} where V_{max} (Volt) is the output voltage of an AE preamplifier. G_{pre} (dB) is the gain of the AE preamplifier.	Figure 10
Hit duration	Hit duration is defined as the time from the first threshold-crossing to the last threshold-crossing of the AE waveform signal.	Figure 10
Hit count	Count is the number of threshold-crossings upward. In the illustration, there are four counts.	Figure 10
Absolute energy	Absolute energy is the energy contained in an AE waveform signal. HD absolute energy = $\int_{T_1}^{T_2} \frac{[V(t)]^2}{R} dt$ where $V(t)$ is the voltage of the AE signal and R is a reference resistance (10kΩ). T_1 and T_2 are the time of the first threshold-crossing and the last threshold-crossing of an AE waveform signal, respectively.	Figure 11
PAC energy	The term "PAC energy" was defined by Physical Acoustics Company (PAC). PAC energy is the integral of the rectified voltage signal over the duration of a single AE event. PAC energy has used this 2-byte energy definition since 1978. The dynamic range is from 0 to 65355 counts. One count (the least significant bit) corresponds to 10 μVsec. The resolution is 1 count.	-
Signal strength	Signal strength is mathematically the same as PAC energy. The differences are dynamic range and resolution. The dynamic range of signal strength is from 0 to 13.1 mVsec. The resolution is 3.05 pVsec.	-
rms	HD RMS is defined as the root mean squared value of the voltage of the AE waveform.	-
Average signal level (asl)	HD ASL is mathematically the same as the RMS. The difference is t he units. While the RMS is represented in V, HD ASL is represented in dB with the reference of 1μV. HD ASL (dB) = 20 log ($V_{rms}/(10^{-6})$) - G_{pre} where V_{rms} (V) is the voltage of an AE waveform signal. G_{pre} (dB) is the gain of the AE preamplifier.	-
Peak frequency	Peak frequency (kHz) is defined as the point at which the peak magnitude occurs in the frequency spectrum. A real time FFT is performed over a single hit.	-
Average frequency	Average frequency (kHz) is defined as the count divided by hit duration.	-
Frequency centroid	Frequency centroid (kHz) is defined as the first moment of inertia of frequency for a single AE event. It is calculated as follows. Frequency centroid = $\sum_{i=1}^{n} Mag_i \times Fre_i$ where Mag_i is the amplitude of i^{th} FFT bin and Fre_i is the frequency of i^{th} FFT bin.	-

Table 2 Definition of AE Time-Driven Feature

rms	TD RMS is defined as the root mean squared value of the voltage of the AE waveform over the entire measurement duration.	-
asl	TD ASL is mathematically the same as the TD RMS. The difference is the units. While the TD RMS is represented in V, TD ASL is repr esented in dB with the reference of 1μV. TD ASL (dB) = 20 log ($V_{rms}/(10^{-6})$) - G_{pre} where V_{rms} (V) is the voltage of an AE waveform signal. G_{pre} (dB) is the gain of the AE preamplifier.	-
Absolute power	TD absolute power is the power of an AE signal over the entire mea surement duration. The entire measurement duration is defined as ti me period between the start and the end of an AE measurement. The equation for calculating TD absolute power is as follows. $\text{TD absolute power} = \frac{1}{T_2 - T_1}\int_{T_1}^{T_2}\frac{[V(t)]^2}{R}dt$ where $V(t)$ is the voltage signal of AE measurement and R is a reference resistance (10kΩ). T_1 and T_2 are the initial and the final time of the AE waveform, respectively.	Figure 12

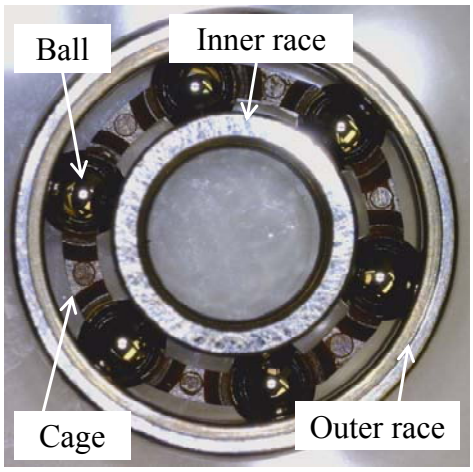

Figure 3 Ball Bearing Used in Tests

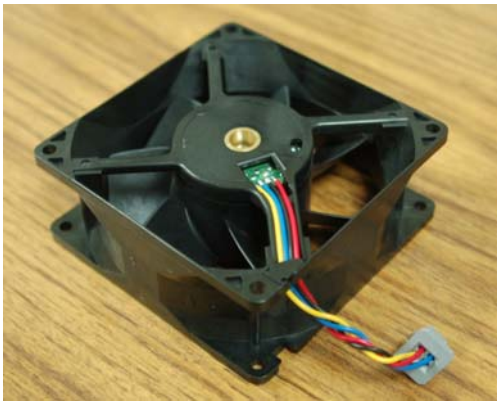

Figure 4 Fan Sample (93 mm × 93 mm × 38 mm)

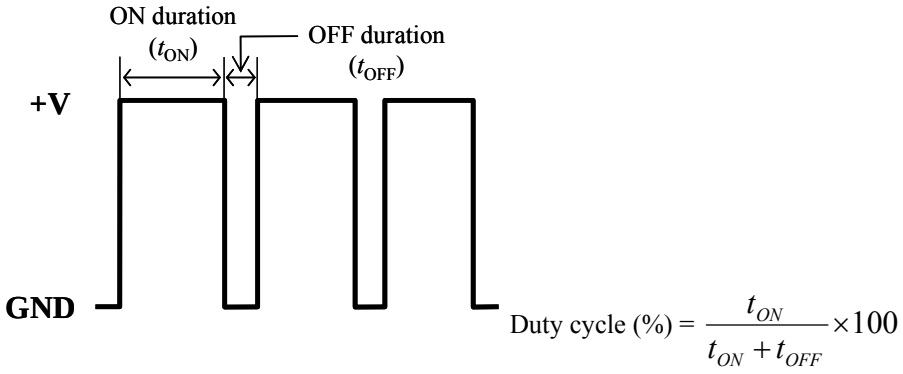

Figure 5 Duty Cycle in Pulse Width Modulation (PWM) Signal

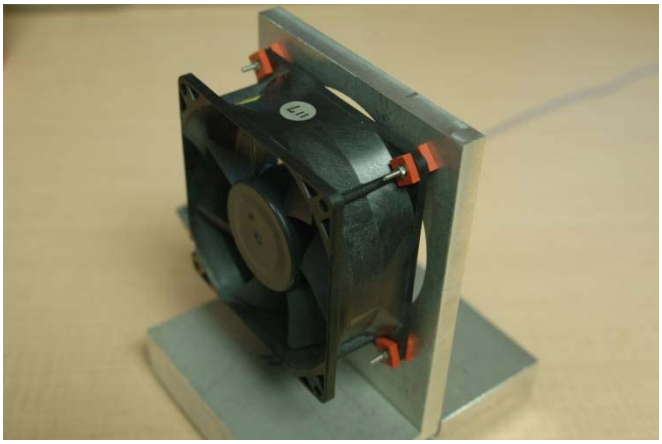

Figure 6 Test Fixture: A Fan is mounted on the test fixture

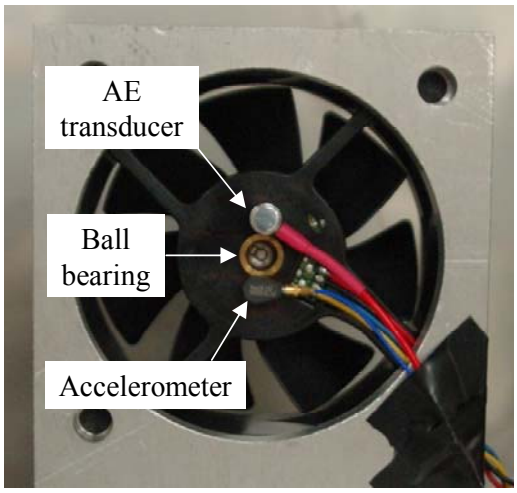

Figure 7 Fan Mounted on Test Fixture with Accelerometer and AE Transducer

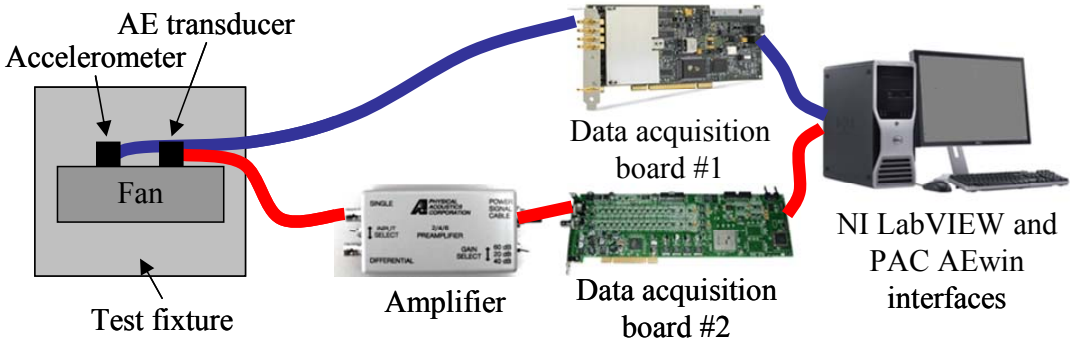

Figure 8 System for Vibration and Acoustic Emission Monitoring

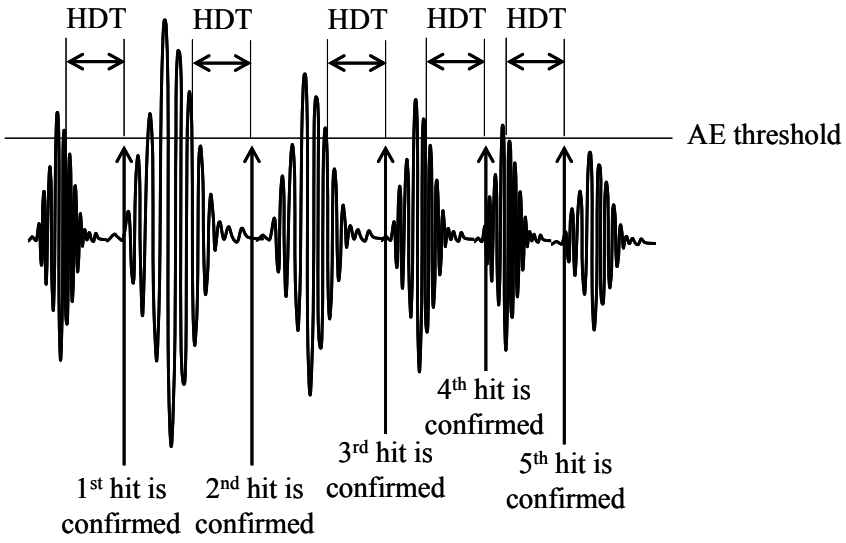

Figure 9 Identification of One Hit by Specified Hit Definition Time

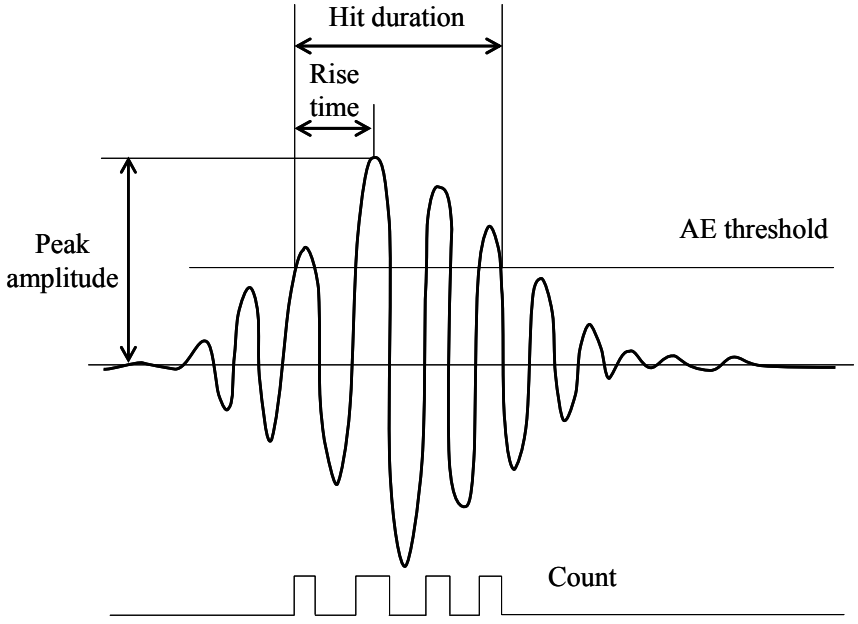

Figure 10 AE HD Feature: Peak Amplitude, Hit Duration, Rise Time, and Hit Count

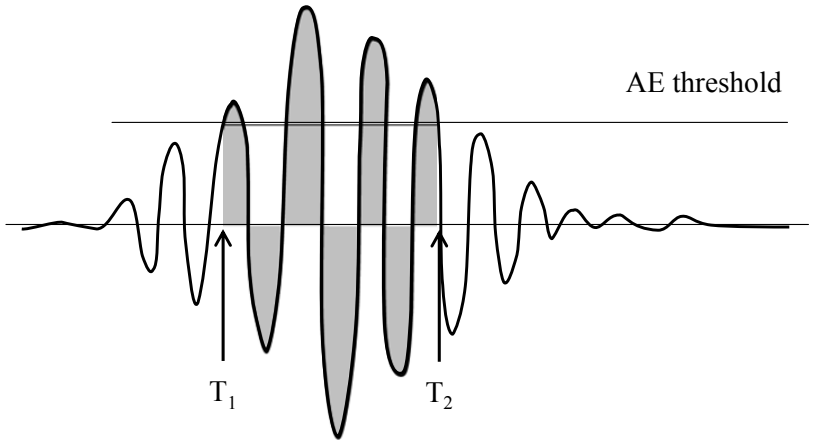

Figure 11 HD Absolute Energy

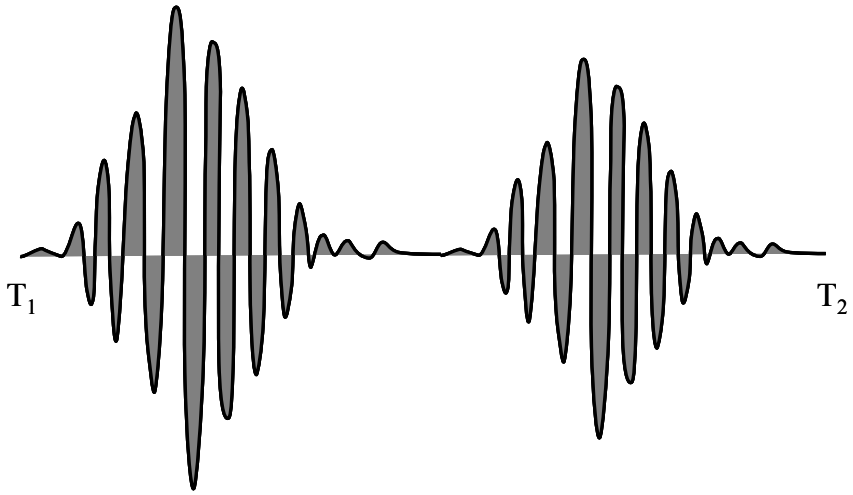

Figure 12 TD Absolute Power

CHAPTER 4 Functional Relationship between Vibration (or Acoustic Emission) and Bearing Defects

This chapter describes the effect of bearing defects formed during stress tests on condition monitoring signals (vibration and AE). Defects in ball bearings were generated by running ball bearings under thermal and mechanical loading conditions below the fatigue load limit rather than seeding defects artificially. Ball bearings operated at 70°C and 4,800 rpm in stress tests. The stress tests continued until the vibration by in situ or periodic measurements exceeds the failure threshold of 22.9 dB from the initial value. Another set of stress tests was terminated before the vibration reached the failure threshold so that conditions of partially degraded ball bearings were identified. The Signals including vibration and AE were characterized at room temperature and 4,000 rpm before starting and after completing the stress tests of the ball bearings. Failure analysis of the ball bearings was conducted using quantitative and qualitative methods to investigate failure mechanism of the ball bearings. The correlation analysis revealed relationship between features extracted from condition monitoring signals (vibration and AE) and defects in ball bearings stressed under thermal and mechanical loading below the fatigue load limit. Figure 13 shows experimental procedures for the correlation analysis.

In the stress test, two types of ball bearing samples were used: ball bearings containing oil and ball bearings containing grease. The details of the preparation of ball bearings were explained in Section 3.1. In the stress test of ball bearings

containing oil, vibration and AE was in situ monitored for ten seconds every 5 minutes. In the stress test of ball bearings containing grease, vibration and AE were periodically measured with a time interval between 10 and 20 days at room temperature. The sampling frequencies of vibration and AE signals were 25.6k samples per second and 1M samples per second, respectively. An example that shows the evolution of vibration and AE of ball bearings with oil is shown in Figure 14 and Figure 15, respectively.

4.1 Failure Analysis

Two identical ball bearings are in a fan to support the rotating shaft of a fan as shown in Figure 16. The bearing A was taken and used for the first and then bearing B was taken and used, even though either of them can be used in failure analysis.

In order to investigate defects in ball bearings, techniques including scanning electron microscopy (SEM) / energy dispersive X-ray spectroscopy (EDS), Fourier transform infrared spectroscopy (FT-IR), and optical surface profilometry. The equipment used for the analysis is Quanta FEG ESEM 200 from FEI Company, Thermo Nicolet 6700, and Wyko NT1100 from Veeco Instrument, Inc.

Procedures for failure analysis of ball bearings are as follows: 1) remove shield plates of a ball bearing; 2) identify any physical damage on the surface of the ball bearing by SEM/EDS; 3) disassemble the ball bearing into bearing elements, including balls, inner and outer races, and a cage; 4) take residual lubricant on the surface of the bearing elements; 5) characterize organic functional groups in residual lubricant by FT-IR; 6) clean the bearing elements in isopropyl alcohol using an

ultrasonic cleaner; 7) mount the bearing elements on a aluminum plate using epoxy; 8) quantify surface roughness of the bearing elements by optical surface profilometry.

For the purpose of control and setting a baseline, unused bearings with oil and unused bearing with grease were investigated. The procedures to conduct the construction analysis of unused bearings are identical to the procedures to conduct the failure analysis of bearings from stress tests.

4.1.1 Surface Characterization

Figure 17 shows the surface of a ball bearing with oil after failure. Debris was found on the surface of bearing elements, while no debris was found on the surface of unused bearings with oil as shown in Figure 18. Isolation of the debris was attempted. However, the size of debris was too small to pick up. The size of debris particles was less than 100 μm. Some of the debris was taken from the surface of the bearing using sticky tape. The debris on sticky tape showed high concentration of carbon. However, the source of the carbon was not distinguishable, since the sticky tape was composed of carbon.

Partially degraded ball bearings with oil that did not fail were investigated. The time duration of partially degraded ball bearings in stress tests (1.0, 7.4, and 18.1 hours) were less than the time duration of failed ball bearings (23.8, 56.3, and 66.2 hours). None of the partially degraded ball bearings exceeded the vibration failure threshold during stress test. In Figure 19, debris was found on the surface of balls stressed for 7.4 hours, while no debris was found on the surface of unused ball bearings as shown in Figure 18.

To understand how quickly the degradation of ball bearings with oil starts, failure analysis of bearings that stressed for one hour. The time duration of one hour was the shortest compared to any other ball bearings that degraded or failed. In Figure 20, debris particles were found on the surface of the ball in the ball bearing. Therefore, it was verified that the degradation of the ball bearings with oil can occur less than one hour.

Bearings with grease after were investigated. The times to failure of the bearings with grease were 320 and 460 days that were much longer than the mean time to failure (48.7 hours) of bearings with oil. The use of grease as a lubricant in bearings extended the life significantly.

In Figure 21 (A), debris was found all around of the surfaces of a ball in the bearings. Figure 21 (B) shows an agglomerate of debris whose size was more than 500 μm, while the size of a ball was 1560 μm. To investigate the source of the debris, the chemical composition of the debris was analyzed as shown in Figure 22 and Table 3. The size of the agglomerate of the debris was enough to be picked up using a tweezer. The agglomerate was located on the surface of a copper tape. The detection of aluminum, silicone, and calcium indicated that some of the debris came from fibers used in a cage to reinforce the cage structure. The detection of iron and silicon indicated that some of the debris came from steel used for balls, inner and outer races. Therefore, the failure analysis of the bearing with grease after failure showed that the debris was a mixture of particles from the cage, balls, and inner and outer races.

The severity of the bearing degradation was not quantified by measuring the amount of debris particles in partially degraded and failed ball bearings. However, the

SEM/EDS analysis of the bearings with oil confirmed that the debris was formed during bearing degradation by thermal and mechanical loading under the fatigue load limit.

4.1.2 Infrared Spectra Analysis

In Figure 23, the IR spectra of the oil taken from unused, partially degraded, and failed bearings were presented. The transmittance of the organic functional group of C=O, C-H, and C-O, increased as the bearings were operated for the longer duration of time at 70°C. Within the wave number range of 1,100 cm^{-1} to 1,300 cm^{-1}, the transmittance of oil taken from unused bearings was lower than the transmittance of oil taken from either partially degraded and failed bearings. The wave number range of 1,100 cm^{-1} and 1,300 cm^{-1} was the range of ester oil that was used in the ball bearing for lubrication. Based on the observations of the trend in the changes of transmittance peaks of the organic functional groups, it is concluded that the oil in ball bearings degraded as the ball bearings operated for a longer time at 70°C.

Figure 24 shows the IR spectra of the grease taken from unused and failed bearings in the stress test. The increase of the transmittance in the organic functional group of C=O, C-H, and C-O was observed from the grease from unused and failed ball bearings. Compared to Figure 23, an additional peak that corresponded to Li-soap (1580 cm^{-1}) was observed. This observation confirmed that the grease contained Li-soap as a thickener. The transmittance of the Li-soap did not show any change between the grease from unused and failed ball bearings. The observation of the trend of C=O, C-H, C-O, and Li-soap showed that the oil from the grease degraded and thickener (Li-soap) did not degrade. Therefore, it was concluded that the ball bearings

with grease degraded by the consumption of oil in the grease such as evaporation rather than oxidation or decomposition of thickener in the grease.

4.1.3 Surface Topology Analysis

Surface profilometry provides a quantitative measure of surface roughness of an object being measured. Since optical surface profilometry does not have any physical contact to the object, the measurement does not change the surface condition before and after the measurement.

The surfaces of bearing elements are not flat. A least square fit to a generalized quadratic equation was used to remove the effect of curved surface in the quantification of surface roughness measurement. The Wyko 1100 Vision 32 software provides options for mapping raw data obtained from the measurement. Equations for given curve fittings are listed in Table 4. A surface profile is calculated by subtracting the curve-fitted (x, y) data from the raw (x, y) data.

The surface topology of a ball from a partially degraded bearing that contained oil is shown in Figure 25. The several spots indicated by red or blue colors indicated that the ball was damaged. However, most of the area indicated by green color was not damaged. Figure 26 shows the surface topology of a ball from a failed bearing. The area of damaged surfaces increased compared to the ball from the partially degraded bearing. Figure 27 shows the surface topology of a ball from a bearing stressed for additional duration of time after its failure. The surface topology of a ball from a failed bearing that contained grease is shown in Figure 28. Uneven surface were observed from all the area on the ball.

Surface roughness can be quantified in terms of surface roughness parameters. Definition, calculation, and use of the surface roughness parameters are shown in Table 5. Average roughness is used for detecting general variations of machined surfaces and for monitoring an established manufacturing process. The use of roughness average (R_a) could be a way for representing the surface condition of degraded bearings [67]. However, R_a does not provide any information on the heights of peaks and valleys, since R_a averages out the peak and valley displacement from a mean line. This limits the use of R_a for characterizing the surface condition of degraded bearings.

Surface finish parameters including maximum profile peak height (R_p), maximum profile valley depth (R_v), and maximum height (R_t) provide information on peak and valley displacement from a mean line. The surface condition of degraded bearings can be described by the surface finish parameters, since they are sensitive to the existence of peaks or valleys. Another parameter is the average maximum profile of the ten greatest peak-to-valley separations in the evaluation area (R_z). R_z is robust on the overall roughness of the surface condition of degraded bearings compared other surface finish parameters, since R_z is not affected by a single highest peak or lowest valley value. Table 6 and Table 7 include results from surface roughness measurements of balls in terms of roughness average (R_a) and maximum height (R_t), respectively. The time to failure of bearings with grease was 7680 hours, while the mean time to failure of bearings with oil was 43.8 hours. The time to failure between the two groups of bearings with different lubricant varied more than two orders of magnitudes. However, the difference between roughness averages of the two groups

of bearings with different lubricant was less than 30%. For maximum height, the difference was less than 40%. The result showed that the use of grease as a lubricant in bearings increased bearing life more than two orders of magnitudes. Table 8 summarizes the results from failure analysis.

4.2 Correlation Analysis

Correlation analysis was conducted to quantify the relationship between vibration (and AE) and defects formed in ball bearings. The correlation was investigated by two steps: 1) extract features from vibration and AE signals characterized at room temperature and 4,000 rpm before and after stress tests of ball bearings; 2) prepare surface roughness results from unused and stressed ball bearings; 3) calculate correlation coefficients between the features and surface roughness results. The ball bearings cannot be reassembled once disassembled. The surface roughness of ball bearings used in stress tests was measured only after the stress test was complete. The surface roughness before starting the stress test of ball bearings was unknown. The surface roughness of the ball bearings before starting stress tests was assumed to be the surface roughness of bearings of another bearing that was not used.

Table 11 shows the rank of vibration features in terms of correlation coefficients between the vibration features and surface roughness of balls in bearings. Peak amplitude showed the highest correlation coefficient (0.731) followed by rms (0.715). However, the difference of the correlation coefficients of the three features was less than 0.02. Table 12 shows the rank of AE features in terms of correlation coefficients between the AE features and surface roughness of balls in bearings. HD

hit count showed the highest correlation coefficient (0.855) followed by hit duration (0.812). The correlation coefficient of HD hit count was the highest among the correlation coefficients of vibration and AE features. In summary, features, including AE hit duration, AE hit duration, vibration peak, and vibration rms, are potential features to detect faults of ball bearings and predict life of ball bearings.

4.3 Sensitivity of Vibration and AE Features to Fault Detection

AE is the generation of elastic waves released from localized sources within a material when the material undergoes deformation. Vibration occurs when a ball passes over defects on the surfaces of other elements. Interactions between wear particles and damaged surfaces were the sources for generating both vibration and AE.

Twenty features were extracted from vibration and acoustic emission signals to compare the sensitivity of features to detection of defects in ball bearings. AE features including AE rise time, AE hit duration, and AE hit count showed early fault detection compared to other vibration and AE features. Therefore, the three AE parameters are potential precursor parameters for bearing failure. AE rise time from ball bearings with oil tested until failure is shown in Figure 29. At time zero, the AE rise time was below 2 msec. At the time of 9.3 hours in the stress test, the AE rise time exceeded 7.1 msec that was 20% increase of the maximum value of AE rise time. AE hit duration showed a similar trend as shown in Figure 30. At the time of 14.7 hours in the stress test, the AE hit duration exceeded 21.0 msec that was 20% increase of the maximum value of AE hit duration. Another AE feature, AE hit count is shown in Figure 31. At the time of 21.2 hours in the stress test, the AE hit count exceeded 2880 counts that were 20% increase of the maximum value of AE hit count. The three

AE features, including AE rise time, hit duration, and hit count, provided early detection of faults in bearings with oil compared to other vibration and AE features. A comparison of fault detection times of ball bearings with oil is shown in Table 9. A comparison of fault detection times of ball bearing with grease is shown in Table 10. The rank for fault detection times were the same for both of bearings with oil and bearings with grease. Therefore, the evolution of vibration and AE in the stress test of ball bearings with oil can be used to understand the evolution of vibration and AE of bearings with grease, even though the bearing life is different more than two orders of magnitudes.

4.4 Summary

Failure mechanism of the ball bearings under thermal and mechanical loading below the fatigue load limit is described as follows: 1) lubricant in the ball bearings physically deteriorated due to evaporation under thermal loading; 2) the degradation of lubricant in bearings led to contacts between asperities on the surfaces of bearing elements; 3) wear particles were generated due to adhesion and breaking of the asperities; 4) the interaction between wear particles and the surface of bearings elements during the rotation resulted in damages on the surfaces of bearing elements.

Correlation between vibration features and surface roughness of balls in bearings was investigated. Vibration peak amplitude and vibration rms showed high correlation (0.731 and 0.715) with surface roughness of unused, partially degraded, and failed ball bearings. Correlation between AE features and surface roughness of balls in bearings was also investigated. AE hit count and hit duration showed high correlation (0.855 and 0.812) with surface roughness of unused, partially degraded,

and failed ball bearings. Those acoustic emission and vibration features were identified to be potential features to detect faults of ball bearings and predict life of ball bearings.

Table 3 Concentration of Debris Taken from Bearing with Grease after Failure

	Concentration (weight %)				
	Spectrum 1	Spectrum 2	Spectrum 3	Spectrum 4	Spectrum 5
Carbon (C)	85.8	40.4	33.1	30.9	34.6
Oxygen (O)	7.3	14.3	26.8	6.0	44.8
Aluminum (Al)	0.1	0.3	5.8	2.8	0.9
Silicon (Si)	0.9	6.8	21.1	18.0	3.9
Phosphorous (P)	-	-	-	1.4	0.0
Calcium (Ca)	0.6	38.3	5.7	40.5	2.6
Iron (Fe)	5.4	-	7.5	0.5	13.1

Table 4 Equation Used for Terms Removal

	Equation
Tilt	$Ax + By + C = z$
Curvature and Tilt	$A(x^2 + y^2) + Bx + Cy + D = z$
Cylinder and Tilt	$Ax^2 + Bxy + Cy^2 + Dx + Ey + F = z$
Sphere	$Ax^2 + By^2 + Cz^2 = 0$

Table 5 Definition, Calculation, and Use of Surface Measurement Parameters [68]

Term	Definition	Calculation
R_a	Roughness average is the main height as calculated over the entire measured length/area.	$Ra = \frac{1}{MN}\sum_{j=1}^{N}\sum_{i=1}^{M}\left\|Z_{ij}\right\|$ Where M and N are the number of data points in X and Y, and Z is the surface height relative to the mean plane.
R_p	Maximum profile peak height is the distance from the mean line/surface to the highest point in the evaluation length/area.	Measured
R_v	Maximum profile valley depth is the distance from the mean line/surface to the highest lowest point in the evaluation length/area.	Measured
R_t	Maximum height is the vertical distance between the highest and lowest points in the evaluation length/area	$R_t = R_p + R_v$
R_z	The average maximum profile of the ten greatest peak-to-valley separations in the evaluation area.	$R_z = \frac{1}{10}\left[\sum_{i=1}^{10} H_i - \sum_{j=1}^{10} L_i\right]$

Table 6 Surface Roughness of Balls in Bearings: Roughness Average (R_a)

			Roughness average (R_a; μm)							
	Bearing condition	Stress duration (hour)	Ball1	Ball2	Ball3	Ball4	Ball5	Ball6	Mean	Peak
Ball bearing with oil	Unused	Not stressed	0.02	0.02	0.02	0.02	0.02	0.02	0.02	0.02
	Before failure	1.0	0.04	0.04	0.05	-	-	-	-	0.04
		7.4	0.02	0.01	0.02	0.01	0.02	0.02	0.02	0.02
		18.1	0.03	0.02	0.02	0.04	0.02	0.04	0.03	0.04
	Onset of Failure	23.8	0.13	0.02	0.08	-	0.10	-	0.08	0.13
		56.3	0.06	0.09	0.09	0.04	0.08	0.18	0.09	0.18
		66.2	0.17	0.18	0.18	0.19	-	0.17	0.18	0.19
	After failure	100	0.19	0.15	0.15	0.12	0.13	0.17	0.15	0.19
		100	-	0.14	0.39	0.26	-	-	0.26	0.39
		100	-	-	0.24	-	-	-	0.24	0.24
Ball bearing with grease	Unused	Not stressed	0.04	0.03	-	-	-	-	0.04	0.04
	Onset of Failure	7,680	0.21	-	-	-	-	0.22	0.22	0.22
		10,560	0.13	0.09	0.09	0.13	-	-	0.11	0.13
		9,120	0.12	0.10	0.26	0.10	0.10	0.18	0.14	0.26

Table 7 Surface Roughness of Balls in Bearings: Maximum Height (R_t)

			Maximum height (R_t; μm)							
	Bearing condition	Stress duration (hour)	Ball1	Ball2	Ball3	Ball4	Ball5	Ball6	Mean	Peak
Ball bearing with oil	Unused	Not stressed	0.19	0.19	0.13	0.23	0.20	0.15	0.18	0.23
	Before failure	1.0	0.39	0.30	0.74	-	-	-		0.74
		7.4	0.20	0.12	0.21	0.12	0.14	0.19	0.16	0.21
		18.1	0.37	0.34	0.25	0.53	0.24	0.43	0.36	0.53
	Onset of Failure	23.8	1.17	0.14	0.85	-	1.05	-	0.80	1.17
		56.3	1.05	0.93	1.28	0.43	1.06	1.26	1.00	1.28
		66.2	1.29	1.36	1.43	1.37	-	1.64	1.42	1.64
	After failure	100	1.63	1.00	1.18	1.14	1.15	1.39	1.25	1.63
		100	-	1.25	2.29	1.70	-	-	1.75	2.29
		100	-	-	2.13	-	-	-	2.13	2.13
Ball bearing with grease	Unused	Not stressed	0.31	0.28	-	-	-	-	0.30	0.31
	Onset of Failure	7,680	1.88	-	-	-	-	1.66	1.77	1.88
		10,560	0.94	0.73	0.67	0.80	-	-	0.79	0.94
		9,120	1.15	1.03	1.48	0.81	0.98	1.07	1.09	1.48

Table 8 Summary of Failure Analysis Results

		Stress duration (hour)	Wear particles	IR spectra	Surface roughness (R_t; μm)
Ball bearing with oil	Unused	Not stressed	Not observed	C=O, C-O, C-H were detected.	0.23
	Before failure	1.0	Observed	The intensity of C=O, C-O, C-H decreased.	0.74
		7.4			0.21
		18.1			0.53
	Onset of Failure	23.8		The intensity of C=O, C-O, C-H further decreased.	1.17
		56.3			1.28
		66.2			1.64
	After failure	100		-	1.63
		100			2.29
		100			2.13
Ball bearing with grease	Unused	Not stressed	Not observed	C=O, C-O, C-H were detected. Li-soap was detected.	0.22
	Onset of Failure	7,680	Observed	The intensity of C=O, C-O, C-H decreased. The intensity for Li-soap did not change.	1.88
		10,560			0.94
		9,120			1.48

Table 9 Comparison of Fault Detection Times of Vibration and AE Features

(Ball Bearings with Oil)

	Fault detection time: time that corresponds to 20% increase compared to peak value in the stress test (% of actual failure time)	Actual failure time
AE rise time	9.3 hours (14.0%)	66.2 hours
AE hit duration	14.7 hours (22.2%)	
AE hit count	21.2 hours (32.0%)	
AE hit-driven rms	31.3 hours (47.3%)	
Vibration rms	40.3 hours (60.9%)	

Table 10 Comparison of Fault Detection Times of Vibration and AE Features

(Ball Bearings with Grease)

	Fault detection time: time that corresponds to 20% increase compared to peak value in the stress test	Actual failure time
AE rise time	40 days (12.5%)	320 days
AE hit duration	60 days (18.8%)	
AE hit count	60 days (18.8%)	
AE hit-driven rms	320 days (100%)	
Vibration rms	320 days (100%)	

Table 11 Rank of Vibration Features in Terms of Correlation Coefficient between Feature and Surface Roughness (R_t)

Vibration feature	Correlation coefficient
Peak amplitude	0.731
rms	0.715
Amplitude at 99.9%	0.639
Crest factor	0.631
Kurtosis	0.550

Table 12 Rank of AE Features in Terms of Correlation Coefficient between Feature and Surface Roughness (R_t)

AE feature	Correlation coefficient
hit count	0.855
hit duration	0.812
rise time	0.777
peak amplitude	0.772
hit-driven root mean square	0.658
time-driven average signal level	0.655
Hit-driven average signal level	0.654
PAC energy	0.654
signal strength	0.654
time-driven root mean square	0.652
average frequency	0.649
absolute power	0.590
absolute energy	0.541
peak frequency	0.532
frequency centroid	0.443

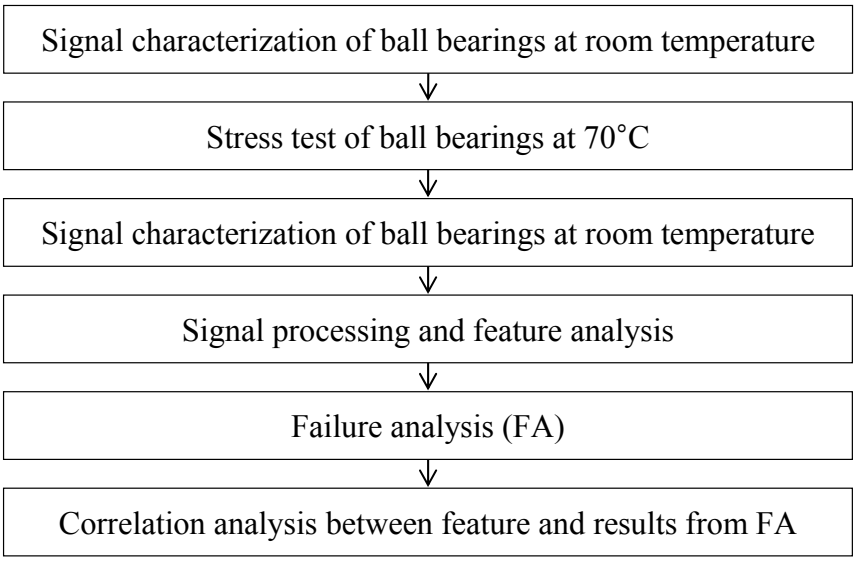

Figure 13 Experimental Procedures

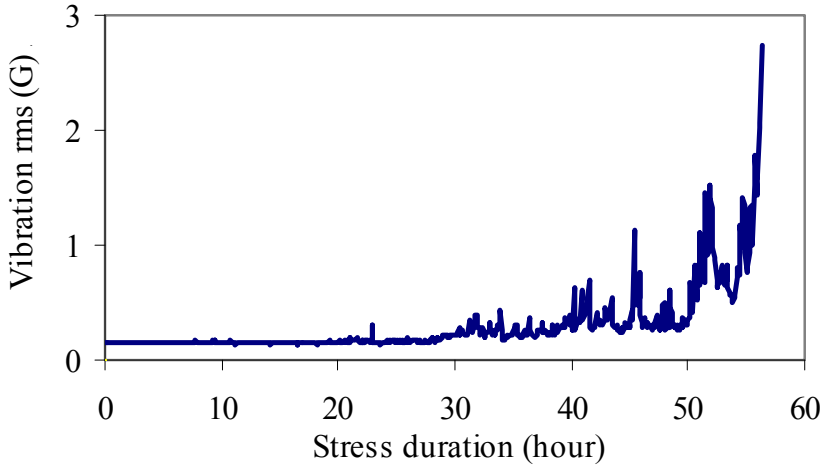

Figure 14 Evolution of Vibration of Ball Bearings with Oil

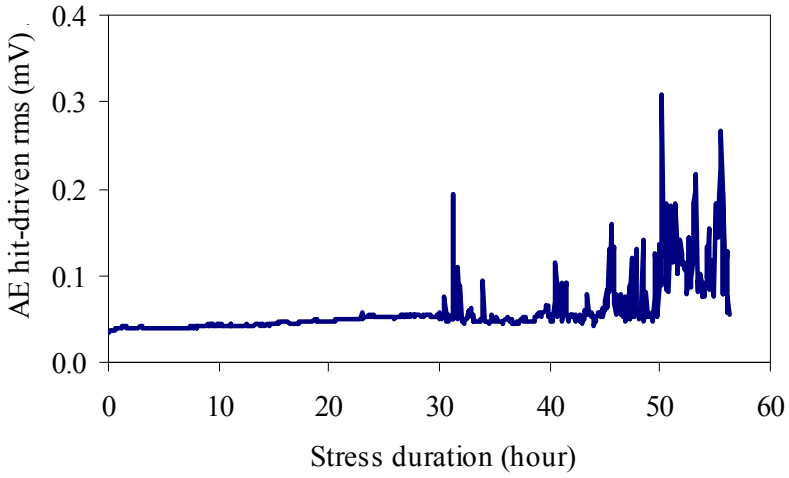

Figure 15 Evolution of AE of Ball Bearing with Oil

(A) Direction of View in the Naming of Bearings

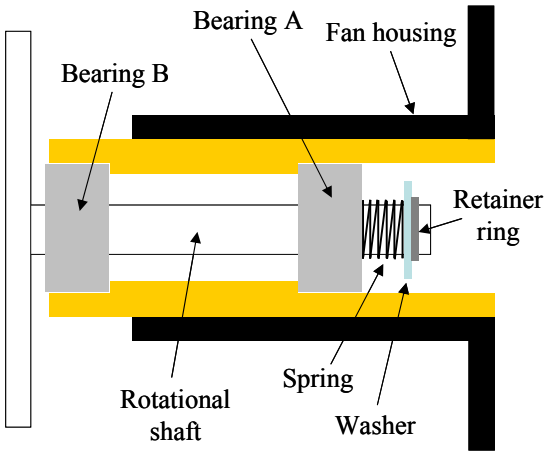

(B) Cross Sectional View of the Fan

Figure 16 Naming Bearing A and B in a Fan

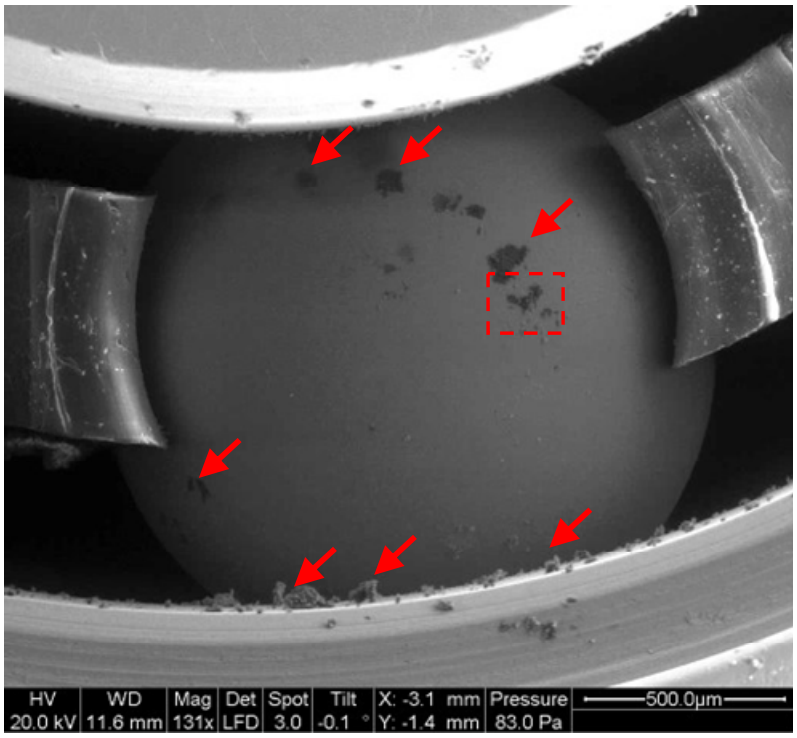

(A) Debris around the Surface of a Ball

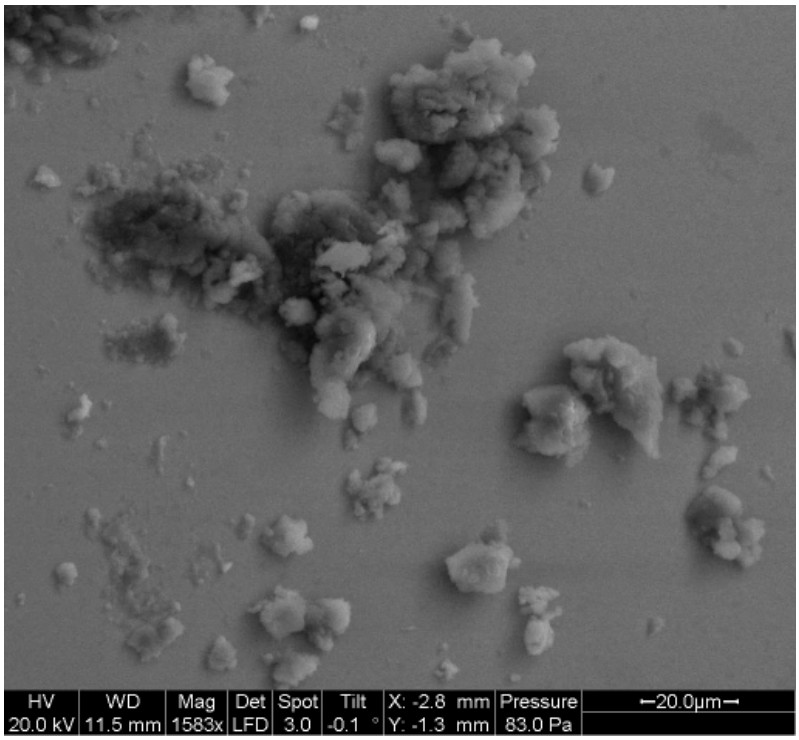

(B) Magnified Image of the Box in (A)

Figure 17 Bearing with Oil (Failure): debris indicated by arrows was found

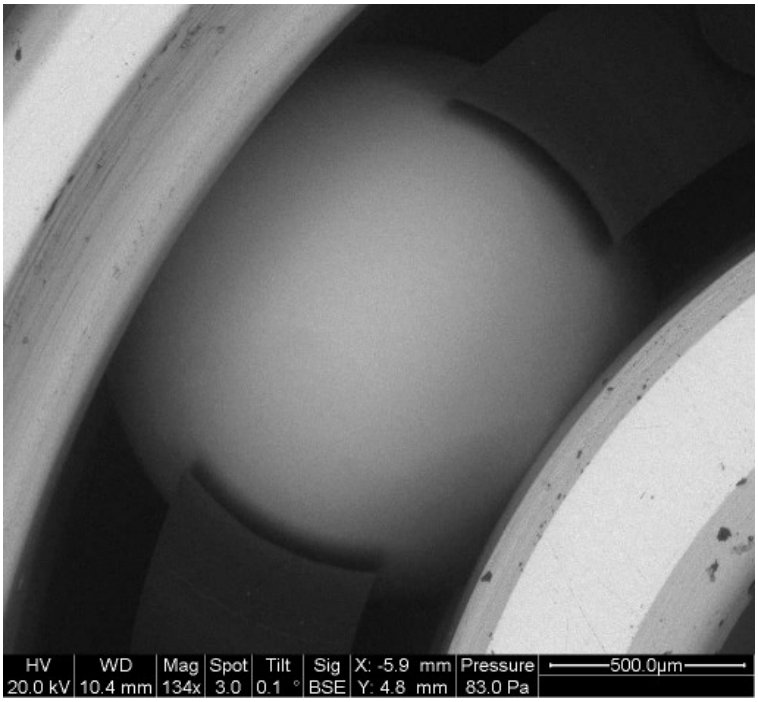

Figure 18 Bearing with Oil (Unused): no debris was found

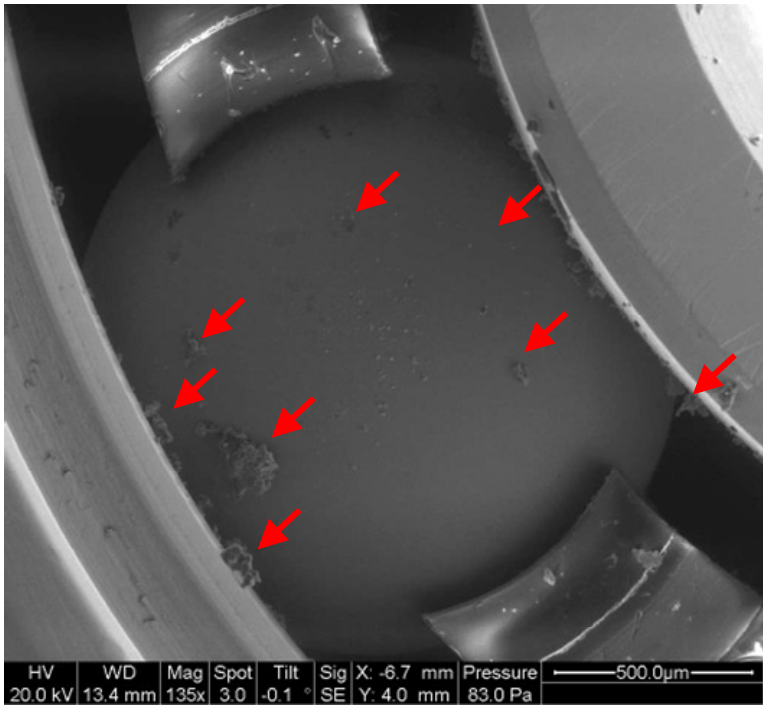

Figure 19 Bearing with Oil (Partially Degraded): debris indicated by arrows was found

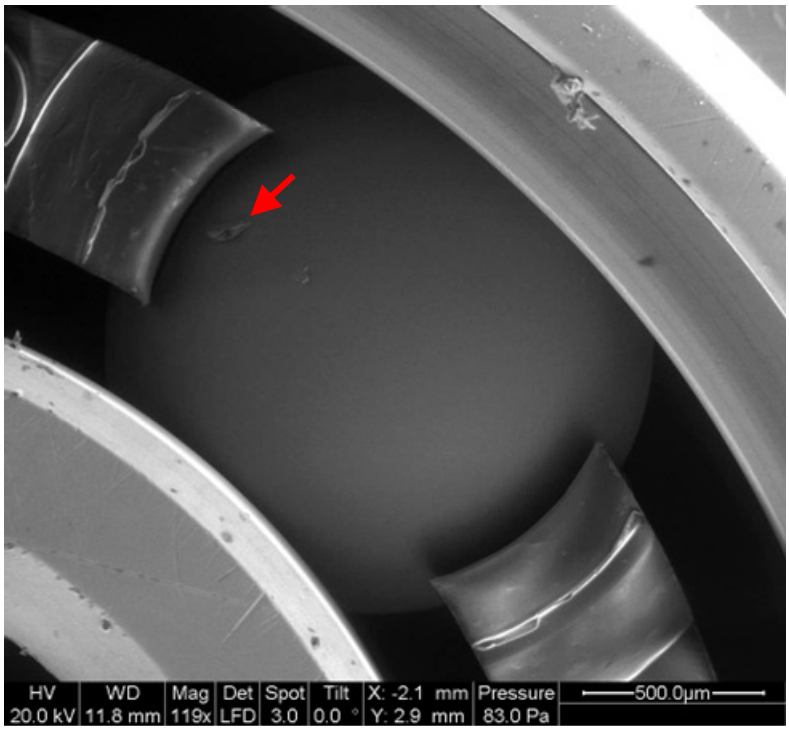

Figure 20 Bearing with Oil (Partially Degraded): debris indicated by arrows was found

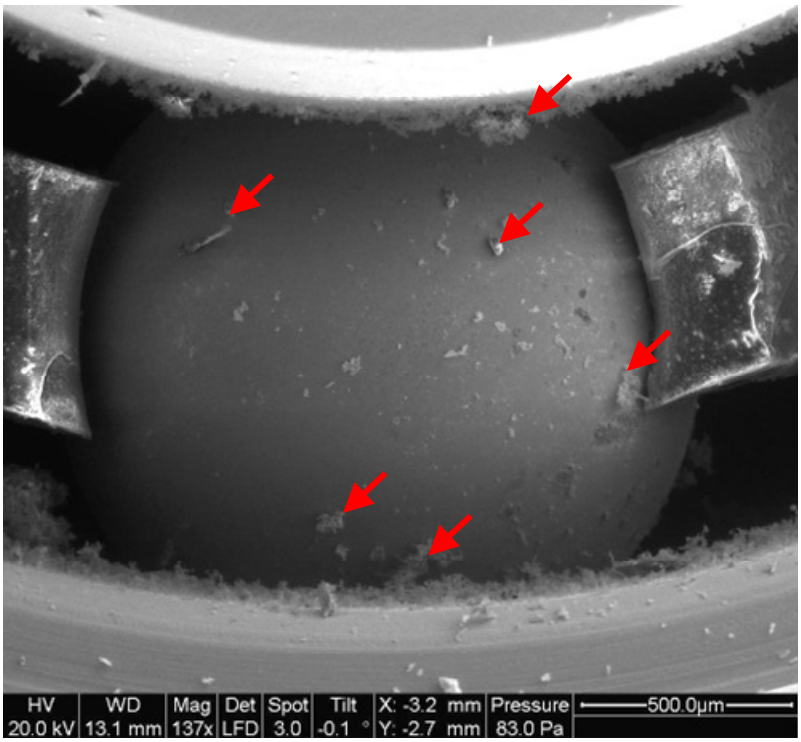

(a) Debris around the Surface of a Ball

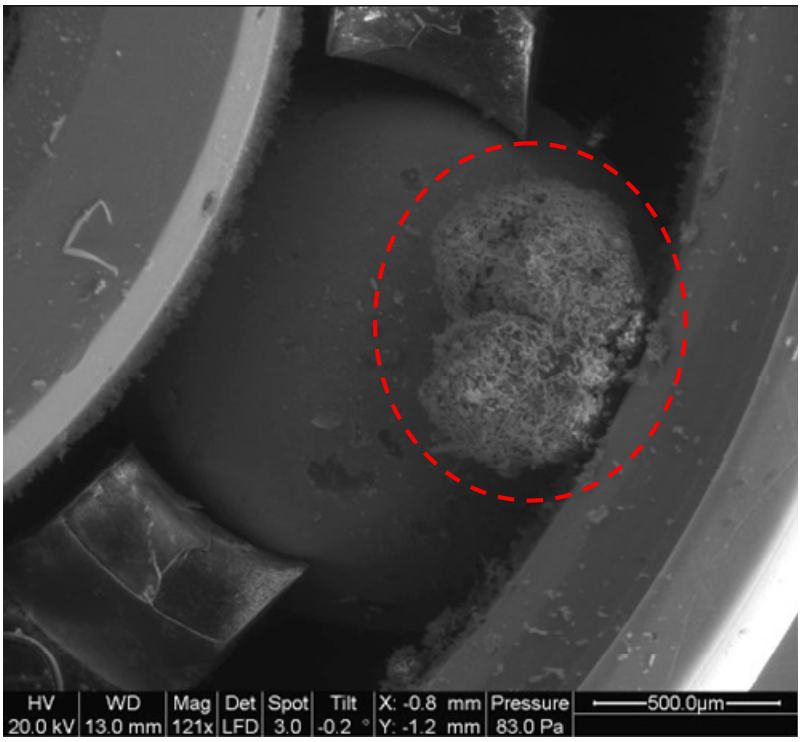

(b) Agglomerate of Debris on the Surface of another Ball

Figure 21 Bearing with Grease (Failed): debris indicated by arrows was found

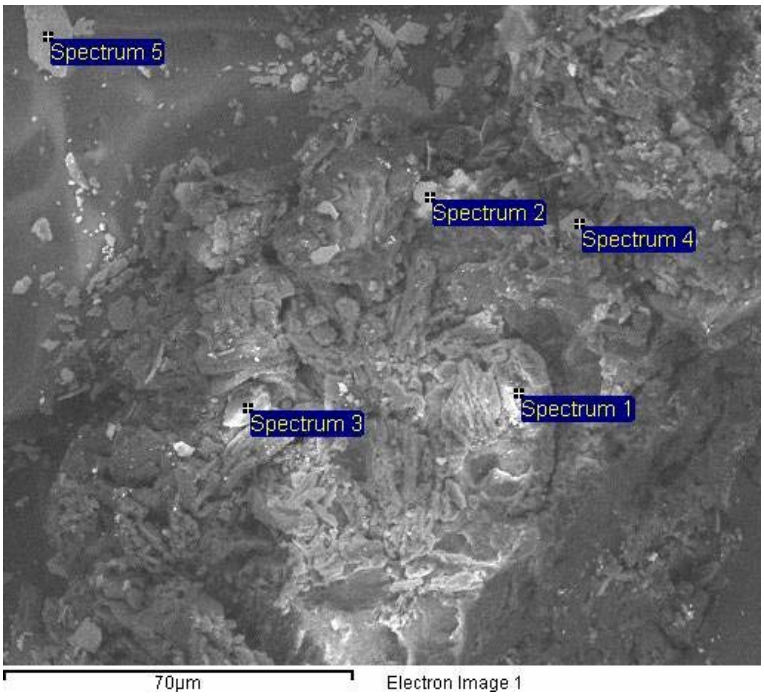

Figure 22 Spots Used for Chemical Concentration Analysis

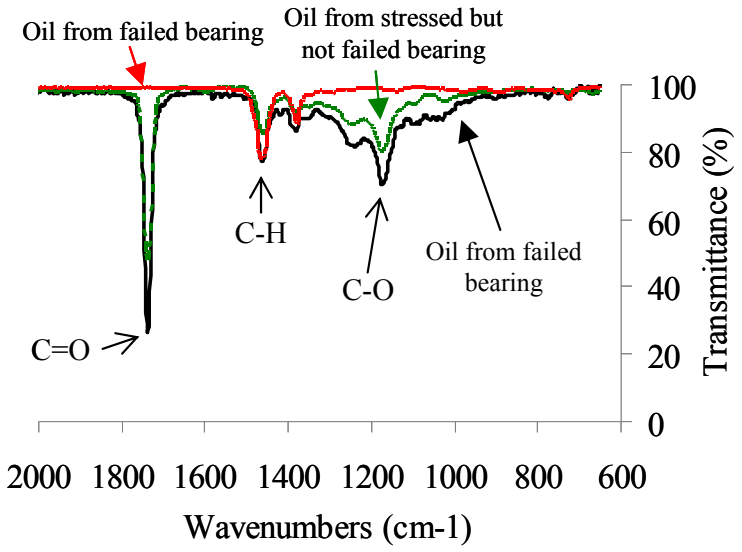

Figure 23 Comparison of Infrared Spectra Using Oil from Unused, Partially Degraded, and Failed Ball Bearings

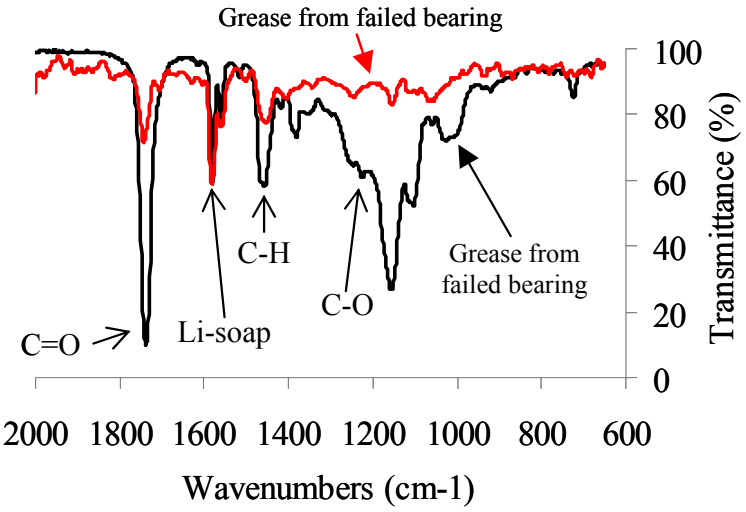

Figure 24 Comparison of Infrared Spectra Using Grease from Unused and Failed Ball Bearings

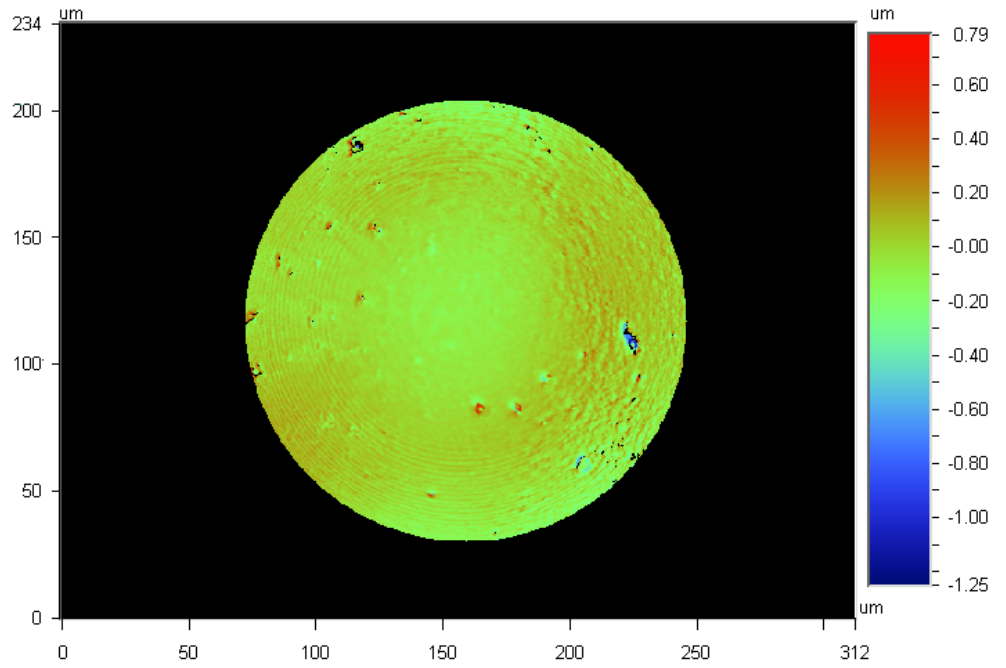

Figure 25 Surface Topology of Ball from Bearing with Oil that Partially Degraded

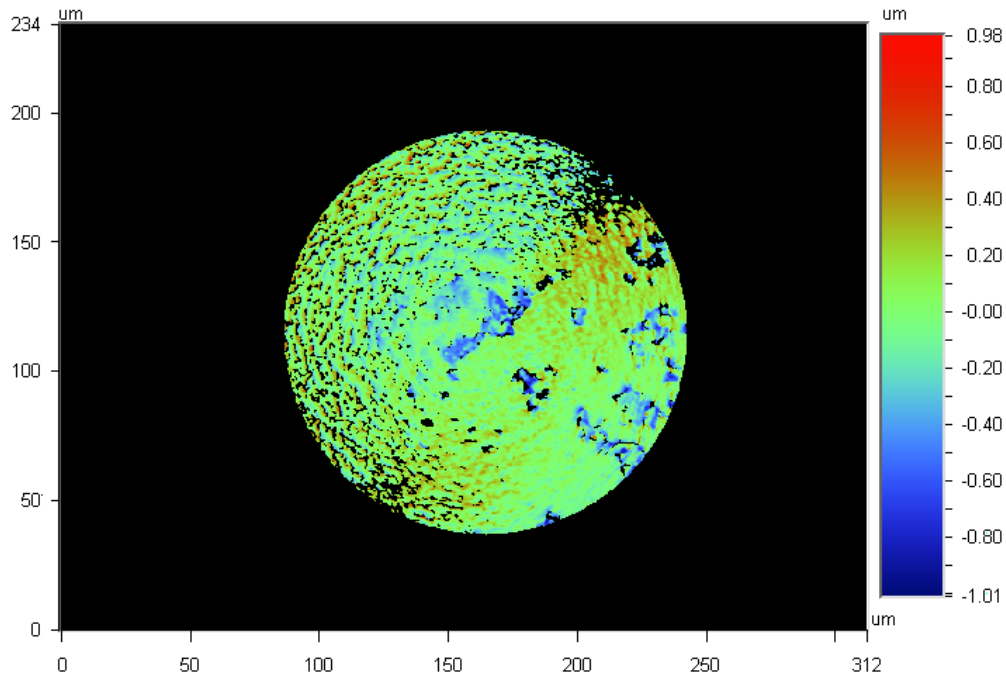

Figure 26 Surface Topology of Ball from Bearing with Oil that Failed

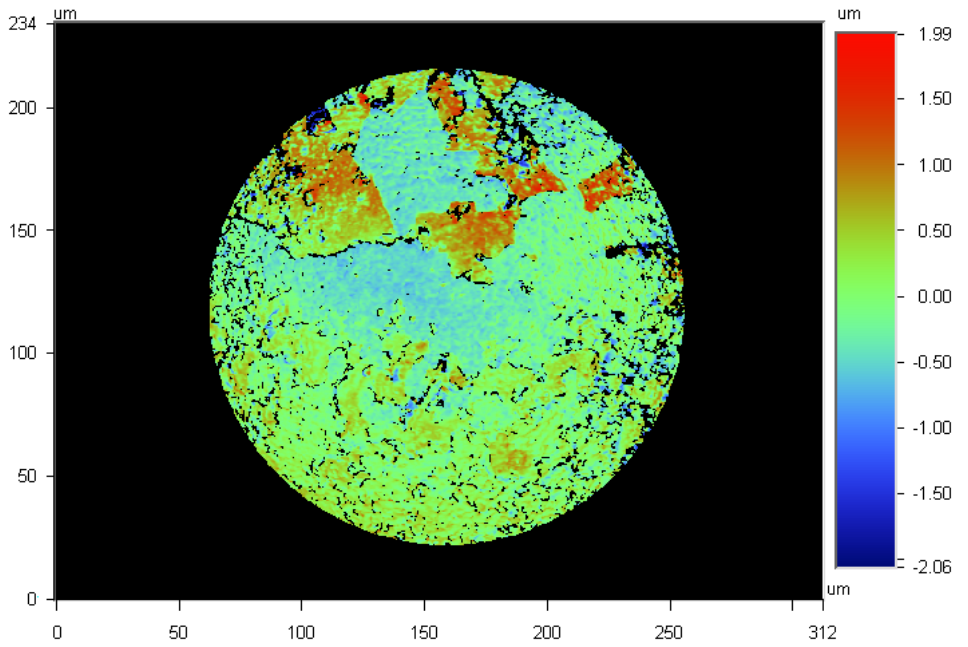

Figure 27 Surface Topology of Ball from Bearing with Oil that Operated after Failure

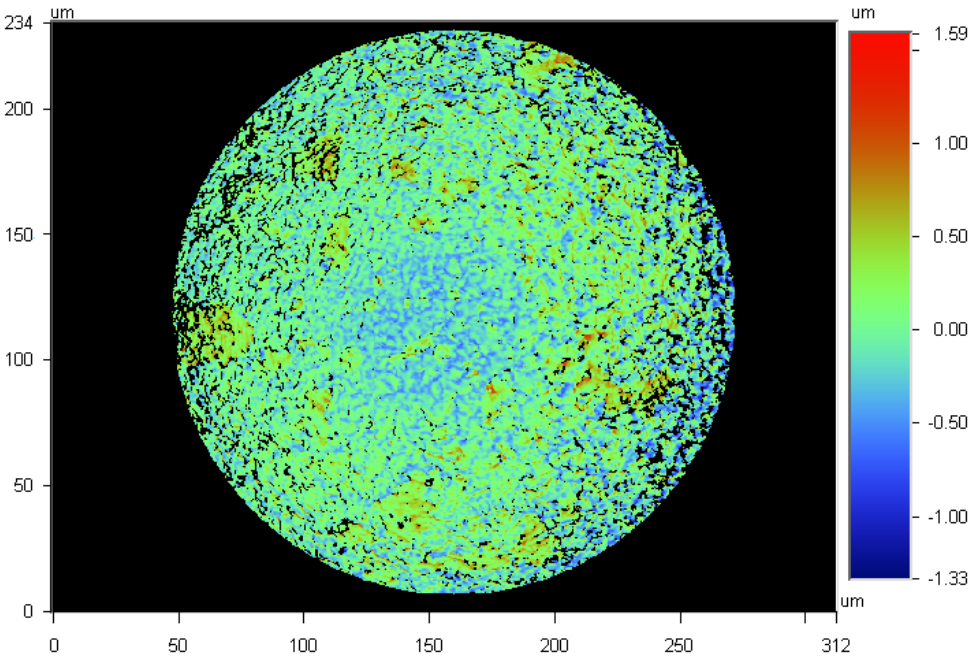

Figure 28 Surface Topology of Ball from Bearing with Grease that Failed

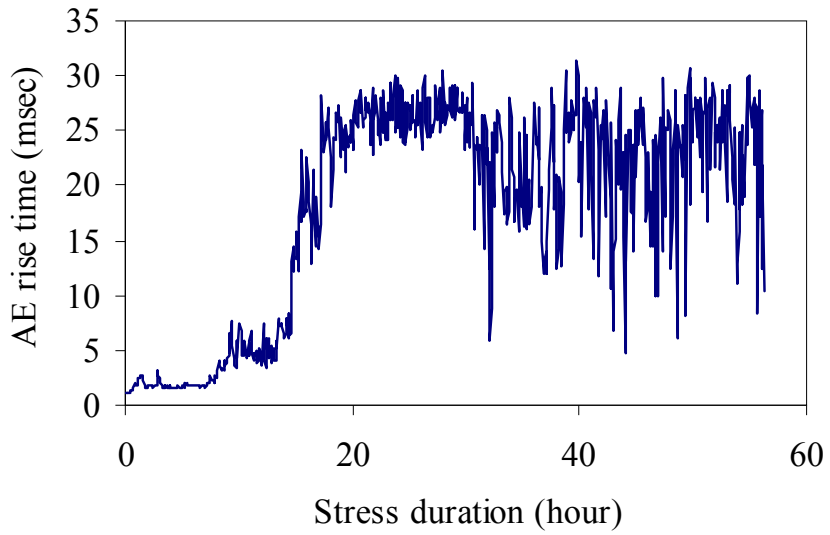

Figure 29 AE Hit-driven Rise Time of Ball Bearings with Oil (failed at 66.2 hours)

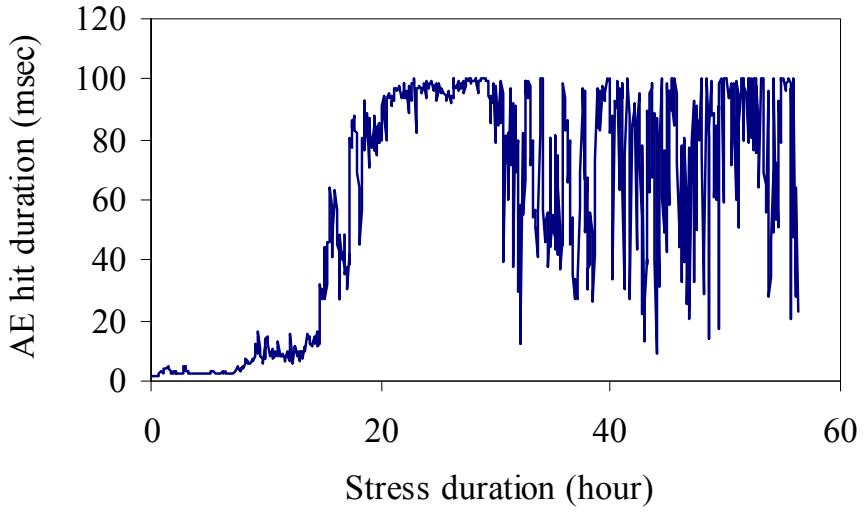

Figure 30 AE Hit-driven Hit Duration of Ball Bearings with Oil (failed at 66.2 hours)

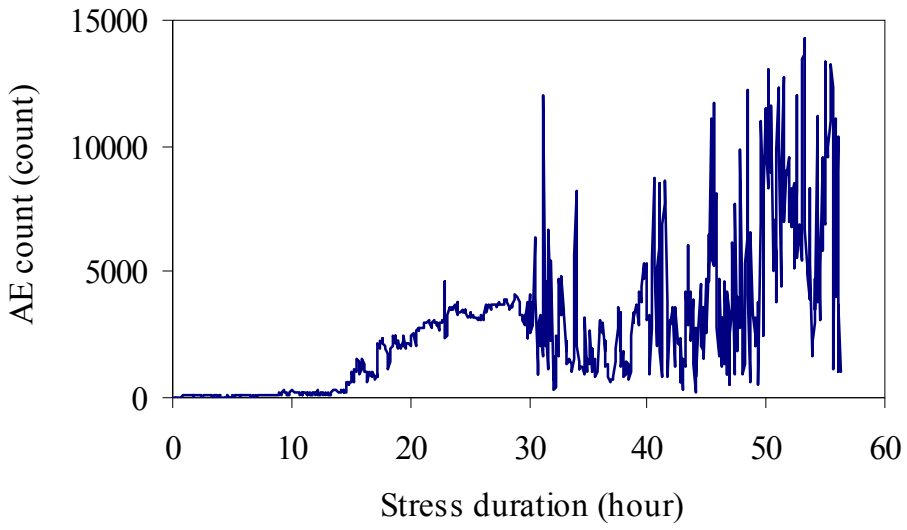

Figure 31 AE Hit-driven Hit Count of Ball Bearings with Oil (failed at 66.2 hours)

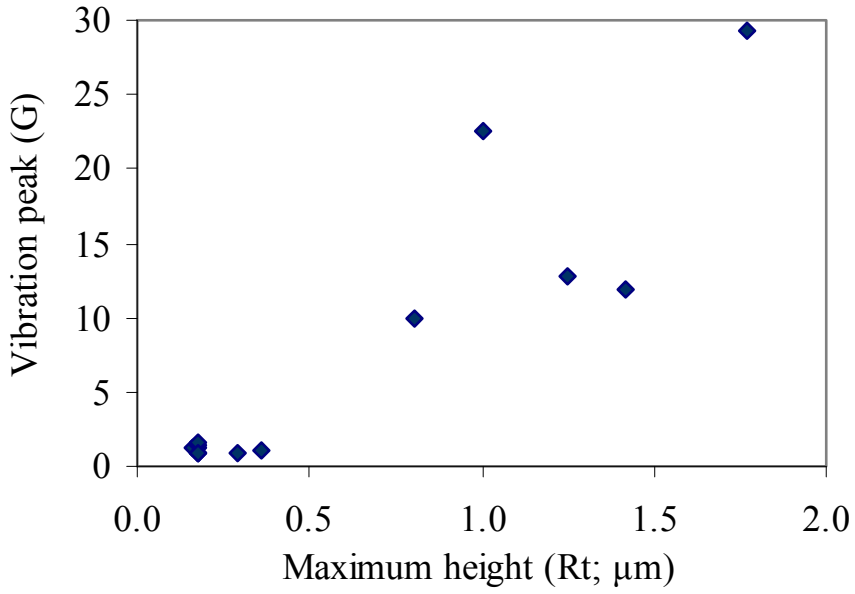

Figure 32 Correlation between Vibration Peak and Surface Roughness (R_t)

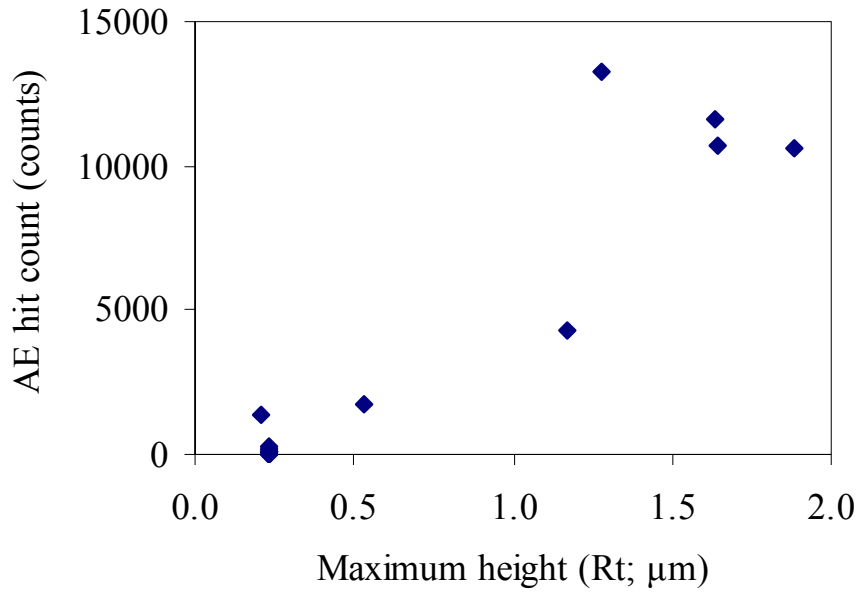

Figure 33 Correlation between AE Hit Count and Surface Roughness (R_t)

CHAPTER 5 Bearing Life Prediction Based on Bayesian Monte Carlo Method and Sequential Probability Ratio Test

This chapter describes the development of a prognostic method of ball bearings from vibration signals using Bayesian Monte Carlo method and sequential probability ratio test. The developed prognostic method is demonstrated using vibration from fan bearings.

5.1 Trending the Evolution of Health Monitoring Index

In order to identify the pattern associated with the bearing degradation, time series of vibration measurements are processed using double exponential smoothing method whose output is a smoothened time series. The effect of vibration measurements collected in the past on the output processed by the smoothing method decreases exponentially. The smoothing method has two equations:

$$s_k = \eta x_k + (1-\eta)(s_{k-1} + b_{k-1}) \qquad \text{Equation 1}$$

$$b_k = \gamma(s_k - s_{k-1}) + (1-\gamma)b_{k-1} \qquad \text{Equation 2}$$

where s is the amplitude of double exponentially smoothened vibration rms. b is the trend of the smoothened time series. x is the vibration rms from stress test of ball bearings. The subscript, k, is the integer that indicates the time step ($k \geq 1$). η and γ are constants in the smoothing equations. For the initial condition of s and b, $s_0 = x_0$ and $b_0 = x_1 - x_0$. In the first smoothing equation, a sum of the amplitude at the time step k-1 and the trend at the time step k-1 is calculated. Then, the output from the first

smoothing equation is calculated by weighting the measurement at the time step *k* and the sum at the time step *k*-1. In the second smoothing equation, the difference between the two measurements at the time steps *k* and *k*-1 is calculated. The second smoothing equation updates the trend at the time step *k* by weighting the difference and the trend at the time step *k*-1.

The evolution of bearing vibration rms after applying the smoothing method to vibration rms is shown in Figure 34. The smoothened vibration rms from the two stress tests of ball bearings showed a similar pattern over the life. Models used to describe the evolution of bearing vibration were discussed by Shao and Nezu [55]: linear model, polynomial model, exponential model, and compound model. For example, a linear model was used to describe the pattern of bearing vibration degraded by lubricant deterioration. An exponential model was used to describe the pattern of bearing vibration degraded by material fatigue [59]. A compound model is a combination of linear and exponential models which is flexible to describe multiple patterns of bearing vibration. In this research, a compound model is used to describe the degradation pattern of smoothened vibration rms.

$$z^{(t)} = a_0 + a_1 t + a_2 \exp(a_3 t) \qquad \text{Equation 3}$$

where, z is the output from the fitted compound model. t is the time. a_1, a_2, and a_3 are the parameters of the compound model.

Figure 35 shows the smoothened vibration rms of bearings in three independent stress tests and compound models fitted to each smoothened vibration rms. R^2 values of the curve fitting were , for the stress test no. 1, no. 2, and no. 3, respectively.

5.2 Parameter Estimation Using Bayesian Monte Carlo Method

There are uncertainties associated with parameters in a compound model to make life prediction of bearings. First of all, bearings are not identical. The geometrical distribution of lubricant in a bearing varies between bearings. The location and amount of impurities in bearing materials are different. Another source of uncertainty is that the compound model may not be the best model to describe the evolution of bearing vibration. The vibration rms does not always follow the path that is specified by the compound model. Third, there are always measurement errors. An accelerometer may give nonlinear response dependent on the frequency excited. Last, variations of environmental conditions of bearings affect the operation of bearings. For example, the temperature in an oven is not perfectly uniform, even though the oven may have an electrical circuit that controls the oven temperature. Therefore, the parameters in a compound model should be estimated to predict the life of a particular bearing of interest.

In this research, parameters in a compound model are estimated using a Bayesian approach. Parameters described in the form of probability distribution are updated as new information such as additional measurements becomes available. To describe the uncertainties in the parameters of a compound model, parameters are specified by normal distribution.

$$a_{0,k} = a_{0,k-1} + w_0 \qquad w_0 \sim N(0, \sigma_0) \qquad \text{Equation 4}$$

$$a_{1,k} = a_{1,k-1} + w_1 \qquad w_1 \sim N(0, \sigma_1) \qquad \text{Equation 5}$$

$$a_{2,k} = a_{2,k-1} + w_2 \qquad w_2 \sim N(0, \sigma_2) \qquad \text{Equation 6}$$

$$a_{3,k} = a_{3,k-1} + w_3 \qquad w_3 \sim N(0, \sigma_3) \qquad \text{Equation 7}$$

where $a_{0,k}$, $a_{1,k}$, $a_{2,k}$, and $a_{3,k}$ are parameters estimated at time step, k. w_0, w_1, w_2, and w_3, follow normal distribution with the zero mean and standard deviation of σ_0, σ_1, σ_2, and σ_3, respectively. A compound model at time step, k, is described:

$$z_k^{(t)} = a_{0,k} + a_{1,k}t + a_{k,2}\exp\left(a_{3,k}t\right) \qquad \text{Equation 8}$$

where t equals $k\Delta t$. Δt is the time interval between the time steps k and k-1.

When new information, s_k, is obtained from measurements, the posterior distribution of the parameters in the compound model can be recursively estimated. For example, He et al. [69] recursively estimated parameters in the empirical model for battery prognostics based on Bayesian Monte Carlo method. Sun et al. [70] inferred parameters of a linear model based on sufficient statistics.

In Bayesian framework, there are two steps for the estimation: prediction and update. In the prediction step, the prior probability distribution of parameters given vibration measurements from time step 0 to k-1, $p(A_k|s_{0:k-1})$ is estimated using the Chapman-Kolmogorov equation.

$$p\left(A_k|s_{0:k-1}\right) = \int p\left(A_k|A_{k-1}\right)p\left(A_{k-1}|s_{0:k-1}\right)dA_{k-1} \qquad \text{Equation 9}$$

where A_k is a vector of parameters of $a_{0,k}$, $a_{1,k}$, $a_{2,k}$, and $a_{3,k}$. $p(A_k|A_{k-1})$ is the probability distribution of parameters at time step k, given parameters at time step k-1. $p(A_{k-1}|s_{0:k-1})$ is the probability distribution of parameters at time step k, given measurements from time step 0 to k-1.

In the update step, the posterior distribution of parameters, $p(A_k|s_{0:k})$ is estimated via Bayes' theorem.

$$p\left(A_k|s_{0:k}\right) = \frac{p\left(A_k|s_{0:k-1}\right)p\left(s_k|A_k\right)}{p\left(s_k|s_{0:k-1}\right)} \qquad \text{Equation 10}$$

where $p(s_k|A_k)$ is the probability distribution of vibration measurement at time step k, given parameters at time step k. $p(s_k|s_{0:k-1})$ is the normalizing constant.

Once initial values for parameters in the compound model are given, the posterior distribution of the parameters can be recursively estimated by repeating prediction and update steps. The recurrent use of Equation 24 and 25 forms the basis to obtain an optimal Bayesian solution. However, the equations cannot be calculated analytically except a few cases such as Kalman filter and Wonham filter, since calculation the equations requires the evaluation of complex high dimensional integrals [72][73]. When the analytical solution is intractable, a technique that implements a recursive Bayesian filter by Monte Carlo simulations provides a way to approximate the optimal Bayesian solution. The key concept of the technique is to represent the posterior distribution by a set of random samples with associated weights and to calculate estimates of the distribution using the samples and weights. The posterior distribution of parameters at time step k can be approximated:

$$p\left(A_k|s_{0:k}\right) \approx \sum_{i=1}^{N} w_k^i \delta\left(A_k - A_k^i\right) \qquad \text{Equation 11}$$

where N is the number of samples used in Monte Carlo sampling. A_k^i is a set of points sampled from the posterior distribution, $p(A_k|s_{0:k})$, by Monte Carlo sampling and associated with i^{th} weight, w_k^i, where $i = 1,\ldots, N$. The weights are normalized so that the sum of weights becomes 1. A_k is the set of distribution means of the parameters at time step k. $\delta(\cdot)$ is the Dirac delta function.

Since the true posterior distribution is unavailable, samples cannot be drawn directly from the posterior distribution. One can use importance sampling method that draws samples from an arbitrarily chosen distribution $q(\cdot)$ called the importance

function. The use of importance sampling enables an unbiased estimate of the posterior distribution [71]. When an importance function $q(\cdot) = p(A_k|A_{k\text{-}1}{}^i)$ is chosen, the corresponding non-normalized weights is [69][73]:

$$w_k^i = w_{k-1}^i p\left(s_k \middle| A_k^i\right) \qquad \text{Equation 12}$$

As the number of samples in Monte Carlo simulation increases, the suboptimal solution approximated by Equation 26 converges towards the true posterior distribution.

5.3 Probability Distribution Estimation Using SPRT

In Section 5.2 the pattern of bearing vibration is described using a compound model whose parameters are estimated by a Bayesian filter based on Monte Carlo simulation. Since the estimation from the compound model approximates smoothened time series of the actual measurements, there exists a difference (d_k) between the actual measurement of vibration ($x_k^{(t)}$) and an estimate ($z_k^{(t)}$) from the compound model. In order to account for the difference, a term (v_k) is incorporated into the compound model.

$$y_k^{(t)} = z_k^{(t)} + v_k^{(t)} = a_{0,k} + a_{1,k}t + a_{2,k}\exp\left(a_{3,k}t\right) + \nu_k \qquad \text{Equation 13}$$

where $a_{0,k}$, $a_{1,k}$, $a_{2,k}$, and $a_{3,k}$ are the posterior distribution estimated using a recursive Bayesian filter by Monte Carlo simulations at time step k. v_k is the Gaussian distribution with the mean of 0 and standard deviation of σ_k.

The probability distribution (v_k) is estimated based on a decision from the sequential probability ratio test (SPRT) developed by Wald [74]. While the classical hypothesis test based on Neyman-Pearson theory makes a decision after collecting a

fixed number of measurements, SPRT was devised to make a decision as a measurement becomes available. The number of sequential measurements used in SPRT is not predetermined, but is the smallest number of measurements until a decision is made. SPRT offers three choices: accept the null hypothesis, reject the null hypothesis, or do not make any decision of accepting or rejecting the null hypothesis until measurements are enough to make a decision.

In this research, an SPRT that detects changes in variance of measurements was used to adapt the probability distribution, i.e., variance test. The null hypothesis of the variance test is that the difference at time step k (d_k) belongs to the probability distribution at time step k-1. When the alternative hypothesis of the SPRT is that the difference at time step k (d_k) belongs to the probability distribution with a larger standard deviation compared to the distribution of noise at time step k-1, an SPRT index for a normal variance test is used and defined:

$$\text{SPRT index} = \frac{\sum_{i=1}^{n}(d_k)^2}{2(\sigma_k)^2}\left(1-\frac{1}{V}\right)-\frac{n}{2}\ln(V) \qquad \text{Equation 14}$$

where, V is the system disturbance magnitude, which is preassigned by the user. n is the number of iterations for SPRT without making any decision. When the alternative hypothesis of the SPRT is that the difference at time step k (d_k) belongs to the probability distribution with a smaller standard deviation compared to the distribution of noise at time step k-1, an SPRT index for an inverse variance test is used and defined:

$$\text{SPRT index} = \frac{\sum_{i=1}^{n}(d_k)^2}{2(\sigma_k)^2}(1-V)-\frac{n}{2}\ln(V) \qquad \text{Equation 15}$$

Figure 36 shows the procedure for adapting the probability distribution to model the difference. The SPRT index is calculated using either normal or inverse variance test. The SPRT index is compared to thresholds, A and B. SPRT uses thresholds based on false alarm rate (α) and missed alarm rate (β) as follows.

$$A = \frac{1-\beta}{\alpha} \qquad \text{Equation 16}$$

$$B = \frac{\beta}{1-\alpha} \qquad \text{Equation 17}$$

If the SPRT index is larger than or equal to A, the null hypothesis is accepted and the standard deviation at time step k (σ_k) is decreased. If the SPRT index is smaller than or equal to B, the null hypothesis is rejected and the standard deviation at time step k (σ_k) is increased. When a decision of accepting or rejecting of the null hypothesis is made from the SPRT, the corresponding SPRT index is reset to zero. Otherwise, the standard deviation at time step k (σ_k) is assigned to the standard deviation at time step k-1 ($\underline{\sigma_k}$).

5.4 Bearing Life Prediction

The Bayesian filter with Monte Carlo simulation uses n number of samples to approximate the posterior probability of the parameters of a compound model. Using a set of points, $A^i_k=\{a^i_{0,k}, a^i_{1,k}, a^i_{2,k}, a^i_{3,k}\}$ associated with the corresponding i^{th} sample, an i^{th} trajectory that describes the bearing degradation is calculated:

$$y_k^{(t),i} = a^i_{0,k} + a^i_{1,k}t + a^i_{2,k}\exp\left(a^i_{3,k}t\right) + \nu_k \qquad \text{Equation 18}$$

where v_k^i is the sample randomly drawn from the probability distribution adapted by SPRT.

Since the failure threshold was defined as the 22.9 dB increase from the initial measurement (x_0), the time-to-cross (TTC^i_k) that i^{th} trajectory crosses the failure threshold is calculated.

$$a^i_{0,k} + a^i_{1,k} TTC^i_k + a^i_{2,k} \exp\left(a^i_{3,k} TTC^i_k\right) + v^i_k = x_0 10^{\frac{22.9}{20}} \qquad \text{Equation 19}$$

The probability distribution of the TTC is approximated:

$$p\left(TTC_k \middle| z_{0:k}\right) \approx \sum_{i=1}^{N} w^i_k \delta\left(TTC_k - TTC^i_k\right) \qquad \text{Equation 20}$$

The time to failure (*TTF*) of bearings are calculated by using the probability of the *TTC*. Since the failure of bearings is determined if a single value of vibration rms exceed the failure threshold, the left-hand side of the probability distribution of the *TTC* is the area used for estimating the *TTF*. The right-hand side of the probability distribution of the *TTC* is not the area of interest. The predicted failure time (t_{PFT}) is defined as follows:

$$t_{\text{PFT}} = P\left(TTC_k \le \eta(p)\right) = \sum_{TTC_k < \eta(p)} \left[\sum_{i=1}^{N} w^i_k \delta\left(TTC_k - TTC^i_k\right)\right] \qquad \text{Equation 21}$$

where $\eta(p)$ is the value on the *TTC* axis such that $100p\%$ of the area under the graph of the probability density of *TTC* lies to the left of $\eta(p)$ and $100(1\text{-}p)\%$ lies to the right. For example, $\eta(0.01)$, the 1^{th} percentile, is such that the area under the graph of the probability density of *TTC* to the left of *TTC* is 0.01. The value of p is determined based on the life prediction results of bearings from training dataset.

5.5 Life Prediction of Ball Bearings in Fans

Vibration of ball bearings in fans was in situ monitored during stress tests. The ball bearing used in the stress test had oil for lubrication of bearing elements.

Stress tests of six fans were conducted. Three of them were used to train the prognostic model.

5.5.1 Parameter Initialization in the Life Prediction Model

Vibration signals from three fans (No. 1 to 3) were used to setup initial values for parameters in the life prediction model. Parameters for the double exponential smoothing were set to be 0.002 (η) and 0.1 (γ). Probability distributions for parameters in the compound model were described by Gaussian distribution with the mean and standard deviation. The mean and standard deviation were obtained from fitting smoothened vibration rms using the compound model as follows: $a_1 \sim N(0.1428, 0.000100)$; $a_2 \sim N(-0.004813, 0.000105)$; $a_3 \sim N(0.03185, 0.001027)$; $a_4 \sim N(0.3796, 0.010340)$.

The numbers of particles used in the Bayesian filter with Monte Carlo simulation was 1,000. The threshold for the resampling was 0.40. Normal variance test in SPRT was used. False positive and negative probabilities were set to 0.01. System disturbance magnitude was set to 2. The value of p was 0.1%.

5.5.2 Results

Table 13 shows predicted failure times and actual failure time for bearings in stress tests. The predictions started when the lifetime of bearings reach 50% of the lifetime. Additional predictions were made with the lifetime interval of 10% until failure. In order to calculate the prediction accuracy, the error between predicted and actual failure times was calculated using the following equation.

$$\text{Prediction error (\%)} = \frac{\left(t_{AFT} - t_{PFT}\right)}{t_{AFT}} \times 100 \qquad \text{Equation 22}$$

where t_{AFT} and t_{PFT} are the actual and predicted failure times, respectively.

The calculated errors are shown in Table 14. The maximum error of the predictions made between 50% and 90% life times in the three stress tests was +28.4%. The plus sign indicates that the predicted failure time was beyond the actual failure time (i.e., overestimation). The minus sign indicates that the predicted failure time was below the actual failure time (i.e., underestimation). An underestimation is better than an overestimation, since an overestimation leads to unexpected failure. When predictions were made at 90% of the life time, prediction errors were less than 16%.

5.6 Summary

A prognostic method for bearings was developed based on Bayesian Monte Carlo method and sequential probability ratio test. The parameters of a compound model were updated using a Bayesian filter with Monte Carlo Simulation. The difference between the output from the compound model and the actual measurement of bearing degradation was modeled using Gaussian distribution with zero mean. The standard deviation of the Gaussian distribution was increased or decreased based on decisions from sequential probability ratio test. The combination of the compound model and Gaussian distribution estimated the evolution of bearing degradation over the life. The life prediction was made by finding the evolution of bearing degradation crosses a failure threshold.

Vibration rms from stress tests of ball bearings was used to evaluate the accuracy of life predictions by the developed method. The prediction started when bearings ran for 50% of the lifetime. The prediction was made every 10% increase of bearing lifetime. The maximum error of the predictions made between 50% and 90% life times in the three stress tests was +28.4%. When predictions were made at 90% of the life time, prediction errors were less than 16%. The method developed in this research can be extended as a general method to predict life of a component or system.

Table 13 Predicted Failure Time and Actual Failure Time

	Predicted failure time (t_{PFT}; hour)					Actual failure time (t_{AFT}; hour)
Lifetime when predictions are made (% lifetime)	50%	60%	70%	80%	90%	
Test no. 1	31.6	32.0	32.3	33.7	33.4	33.9
Test no. 2	71.6	63.2	57.9	58.5	62.0	66.2
Test no. 3	22.2	28.1	27.5	26.6	25.2	21.9

Table 14 Prediction Error

	Prediction error (%) $= \frac{(t_{AFT} - t_{PFT})}{t_{AFT}} \times 100$				
Lifetime when predictions are made (% lifetime)	50%	60%	70%	80%	90%
Test no. 1	-6.8%	-5.5%	-4.7%	-0.7%	-1.4%
Test no. 2	+8.2%	-4.6%	-12.6%	-11.7%	-6.4%
Test no. 3	+1.5%	+28.4%	+25.6%	+21.7%	+15.3%

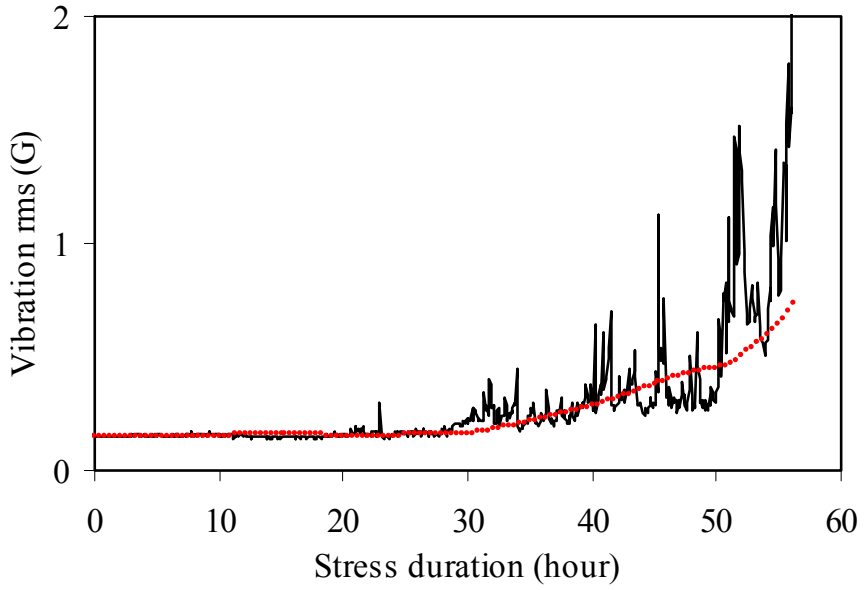

Figure 34 Vibration rms from Stress Tests of Bearings (Black Line) and Smoothened Vibration rms (Red Dots)

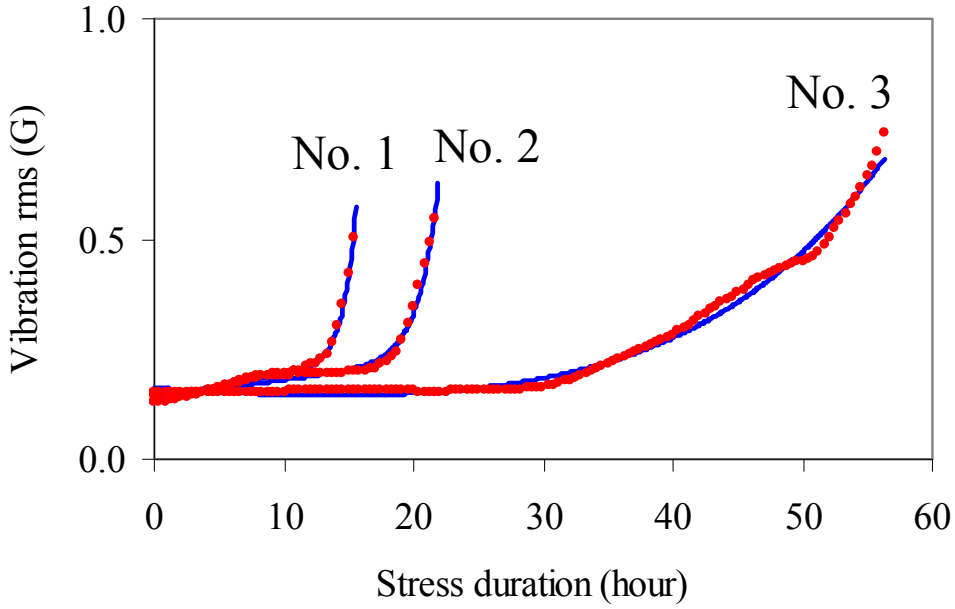

Figure 35 Smoothened Vibration rms (Red Dots) and Fitting of the Vibration rms Using Compound Model (Blue Lines)

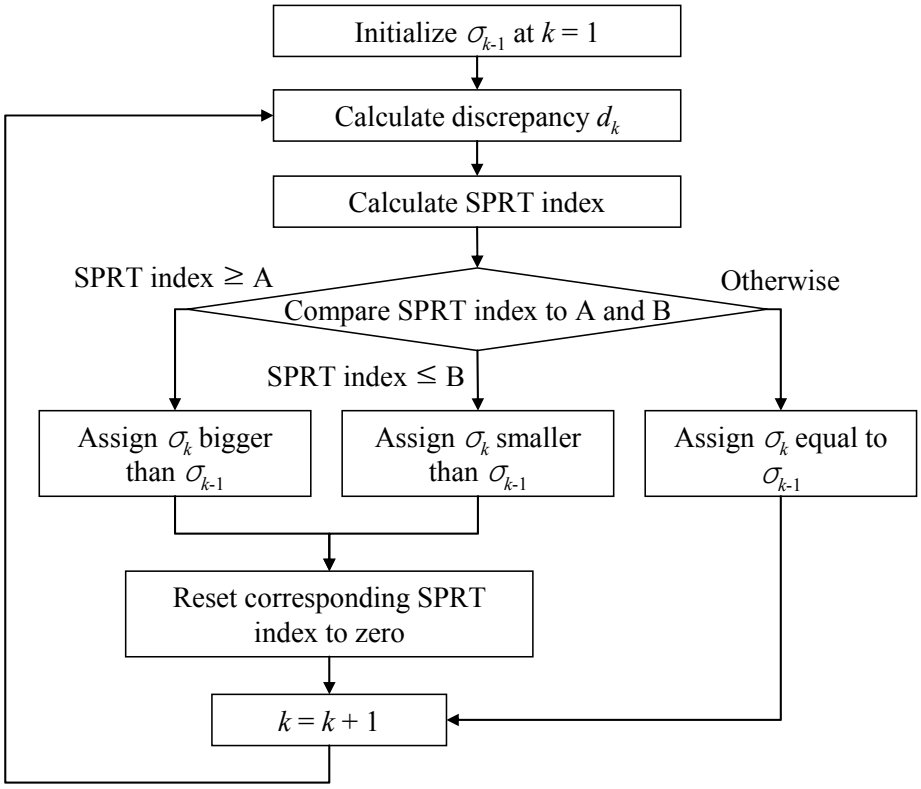

Figure 36 Flowchart to Adapt Probability Distribution Using SPRT

CHAPTER 6 Contributions and Future Work

The contributions of this research are as follows:

- Developed a prognostic method based on Bayesian Monte Carlo method and sequential probability ratio test.
    - Demonstrated life prediction of fan bearings using vibration data collected from life testing of fans operated at an elevated temperature. When predictions were made at 90% of bearing life, errors were less than 16% of total life.
- Determined and quantified a functional relationship between AE hit count and surface roughness of ball bearings operating thermal and mechanical loading below the fatigue limit.
    - Identified the correlation coefficient between AE hit count and the surface roughness of balls in bearings: 0.855.
    - Acoustic emission hit duration provided fault detection of ball bearings as early as 13% of the total life.
- Identified the evolution of vibration and AE of bearings in life testing under thermal and mechanical loading below the fatigue limit of bearings.

Future work may include the following:

- Develop a decision making method that utilizes information obtained from bearing fault detection and life prediction. The ultimate goal for detecting

bearing faults and predicting bearing life is to improve product qualification and/or condition-based maintenance.

- Develop a method to evaluate the uncertainty of life predictions made by the Bayesian Monte Carlo method and sequential probability ratio test.
- Investigate the use of acoustic emission to bearing life prediction. Acoustic emission provides early detection of bearing faults. Acoustic emission may provide higher accuracy than vibration for bearing prognostics.

Appendix

A. Determination of Failure Criterion

The vibration failure criterion for fans in electronic applications was not developed, yet. Even though industrial standards including ECMA-275 [75] and ISO 10302 [66] provides vibration measurement methods for fans in electronics applications, the standards do not specify a vibration failure criterion. The failure of fans was determined based on the failure modes such as decrease of fan speed, increase of electrical current consumption or acoustic noise. Table 15 summarizes the failure modes and corresponding threshold in IPC-9591 [76]. For example, a fan is determined to fail when the increase of audible sound of a fan exceeds 3 dB from its initial value. Since, this study aims to assess the degradation of fans and determine the failure of fans based on vibration signals, a vibration failure criterion for fans is required. Therefore, a vibration failure criterion was developed using correlation analysis between the sound and vibration signals of fans.

Six fans with bearings containing oil were used in the correlation analysis. Audible sound and vibration of a fan was measured for 10 seconds at room temperature and the rated speed of the fan (4,800 rpm). Then the fan was stressed at 70°C. After the stress test, the fan was cooled down to room temperature. The measurement of audible sound and vibration the fan was repeated at room temperature and the rated speed of the fan. The vibration signal was processed using a bandpass filter with the frequency range of 10 Hz to 12.8 kHz and the rms of the

bandpass-filtered vibration signal was extracted. The acoustic signal was processed using A-weighted filter.

Figure 37 shows the relationship between vibration rms and A-weighted sound. The vibration rms equivalent to 3 dBA using the data from the six fans was 22.9 dB with 1mG reference. The standard deviation of errors between the fitted linear line and each measurement data points was 3.8 dB. Therefore, the vibration failure criterion for fans in electronics applications is defined as the 22.9 dB increase from an initial value. The confidence boundary for the vibration failure criterion was ± 7.6 dB with the confidence level of 95%.

We also conducted the correlation analysis using vibration and audible sound data of the same six 0% fans measured with the fan speed of 4,000 rpm. The measurement of vibration and audible sound at 4,000 rpm was conducted after conducting the measurement at 4,800 rpm. The vibration and audible sound was processed in the same way. The vibration rms equivalent to 3 dBA using the data from six 0% fans was 17.1 dB with 1mG reference. The confidence boundary for the vibration failure criterion was ± 8.6 dB with the confidence level of 95%.

Table 15 Failure Criteria of Fans in IPC-9591 [76]

1	Rotational speed reduction	15% decrease of the initial value
2	Increased current consumption	15% increase of the initial value
3	Acoustic noise emission	3 dB increase from the initial value
4	Incorrect or erratic operation of electronic interface	Subjective (not specified)
5	Visible cracking of housing, guards, or impeller parts	
6	Visible leakage of grease/oil or loose bearing seals	

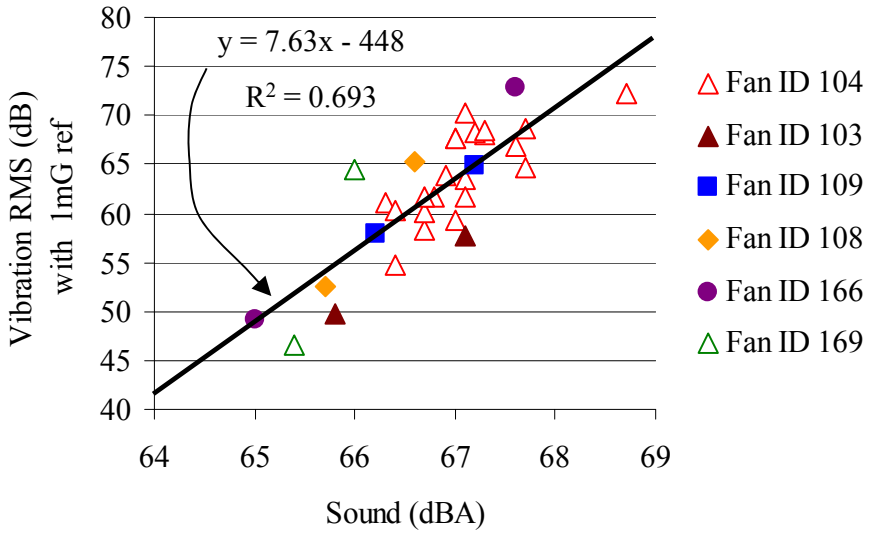

Figure 37 Ball Bearing Used in Tests

References

[1] B.A. Carr, “Kaydon Settles Final Sikorsky Helicopter Crash Litigation,” eBearing Inc., www.ebearing.com/news2001/news199.htm.

[2] S. Kim, C. Vallarino, and A. Claassen, “Review of fan life procedures,” International Journal of Reliability, Quality, and Safety Engineering, Vol. 3, No. 1, pp. 75–96, 1996.

[3] X. Tian, “Cooling fan Reliability: Failure Criteria, Accelerated Life Testing, Modeling and Qualification,” In Proceeding of the Reliability and Maintainability Symposium 2006 (RAMS), pp. 380–384, 2006.

[4] S. Nandi, H.A. Toliyat, and X. Li, “Condition Monitoring and Fault Diagnosis of Electrical Motors A Review,” IEEE Transactions on Energy Conversion, Vol. 20, No. 4, pp. 719–729, 2005.

[5] S. Cheng, M. Azarian, and M. Pecht, “Sensor Systems for Prognostics and Health Management,” Sensors, Vol. 10, pp. 5774–5797, 2010.

[6] ISO 281: Rolling Bearings—Dynamic Load Ratings and Rating Life, Second Edition, International Organization for Standardization, Geneva, Switzerland, February 15, 2007.

[7] T. Harris, Rolling Bearing Analysis, Wiley-Interscience, Fourth Edition, pp. 993–996, New York, NY, 2006.

[8] N. Tandon and A. Choundhury, “A Review of Vibration and Acoustic Measurement Methods for the Detection of Defects in Rolling Element Bearings,” Tribology International, Vol. 32, No. 8, pp. 469–480, 1999.

[9] P. Moore, Nondestructive Testing Handbook, Vol. 6: Acoustic Emission Testing, Third Edition, American Society of Nondestructive Testing, p. 32, p. 243, 2005.

[10] The New York Times, "National News Briefs; Marines Ground Osprey and 363 Helicopters," www.nytimes.com/2000/08/28/us/national-news-briefs-marines-ground-osprey-and-363-helicopters.html, August 28, 2000.

[11] B. James, "Emergency Landings Are Cited: Asia Airbus to Get Change in Engine," The New York Times, www.nytimes.com/1997/05/24/news/24iht-rolls.t.html, May 24, 1997.

[12] SKF Reliability Systems, "Condition Monitoring of Smaller Less Critical Equipment Provides Major Improvements in Reliability and Lower Maintenance Costs," SKF Technical Paper CM1003, www.skf.com/reliability, 2005.

[13] N. Gebraeel, M. Lawley, R. Li, and J. Ryan, "Residual-life Distributions from Component Degradation Signals: A Bayesian Approach," IIE Transactions, Vol. 37, pp. 543–557, 2005.

[14] Dataset from IEEE PHM Data Challenge 2012, http://www.phmconf.org/phm_data_challenge.htm, FEMTO-ST Institute, Besancon, France, 2012.

[15] T. Williams, X. Ribadeneira, S. Billington, and T. Kurfess, "Rolling Element Bearing Diagnostics in Run-to-Failure Lifetime Testing," Mechanical Systems and Signal Processing, Vol. 15, pp. 979–993, 2001.

[16] T. Karacay and N. Akturk, "Experimental Diagnostics of Ball Bearings Using

Statistical and Spectral Methods," Tribology International, Vol. 42, pp. 836–843, 2009.

[17] A.M. Al-Ghamd and D. Mba, "A Comparative Experimental Study on the Use of Acoustic Emission and Vibration Analysis for Bearing Defect Identification and Estimation of Defect Size," Mechanical Systems and Signal Processing, Vol. 20, pp. 1537–1571, 2006.

[18] N. Tandon, G.S. Yadava, and K.M. Ramakrishna, "A Comparison of Some Condition Monitoring Techniques for the Detection of Defect in Induction Motor Ball Bearings," Mechanical Systems and Signal Processing, Vol. 21, pp. 244–256, 2007.

[19] N. Tandon, K.M. Ramakrishna, and G.S. Yadava, "Condition Monitoring of Electric Motor Ball Bearings for the Detection of Grease Contaminants," Tribology International, Vol. 40, pp. 29–36, January 2007.

[20] M. Craig, T.J. Harvey, R.J.K. Wood, K. Masuda, M. Kawabata, and H.E.G. Powrie, "Advanced Condition Monitoring of Tapered Roller Bearings, Part I," Tribology International, Vol. 42, pp. 1846–1856, 2009.

[21] D. Mba and R.B.K.N. Rao, "Development of Acoustic Emission Technology for Condition Monitoring and Diagnosis of Rotating Machines; Bearings, Pumps, Gearboxes, Engines and Rotating Structures," The Shock and Vibration Digest, Vol. 38, pp. 3–16, 2006.

[22] S. Al-Dossary, R.I.R. Hamzah, and D. Mba, "Observations of Changes in Acoustic Emission Waveform for Varying Seeded Defect Sizes in a Rolling Element Bearing," Applied Acoustics, Vol. 70, pp. 58–81, 2009.

[23] H. Oh, T. Shibutani, and M. Pecht, “Precursor Monitoring Approach for Reliability Assessment of Cooling Fans” Journal of Intelligent Manufacturing, Vol. 23, pp.173–178, 2012.

[24] B. Trajin, J. Regnier, and J. Faucher, “Comparison between Stator Current and Estimated Mechanical Speed for the Detection of Bearing Wear in Asynchronous Drives,” IEEE Transactions on Industrial Electronics, Vol. 56, pp. 4700–4708, 2009.

[25] J. Sun, R.J.K. Wood, L. Wang, I. Care, and H.E.G. Powrie, “Wear Monitoring of Bearing Steel Using Electrostatic and Acoustic Emission Techniques,” Wear, Vol. 259, pp. 1482–1489, 2005.

[26] A. Hase, M. Wada, and H. Mishina, “The Relationship between Acoustic Emissions and Wear Particles for Repeated Dry Rubbing,” Wear, Vol. 265, pp. 813–839, 2008.

[27] Z. Rahman, H. Ohba, T. Yoshioka, and T. Yamamoto, “Incipient Damage Detection and its Propagation Monitoring of Rolling Contact Fatigue by Acoustic Emission,” Tribology International, Vol. 42, pp. 807–815, 2009.

[28] T.H. Loutas, D. Roulias, E. Pauly, and V. Kostopoulos, “The Combined Use of Vibration, Acoustic Emission, and Oil Debris on-line Monitoring towards a More Effective Condition Monitoring on Rotating Machinery,” Mechanical Systems and Signal Processing, Vol. 25, pp. 1339–1352, 2011.

[29] S. Lingard and K.K. Ng, “An Investigation of Acoustic Emission in Sliding Friction and Wear of Metal,” Vol. 130, pp. 367–379, 1989.

[30] K. Kida, T. Yamazaki, M. Shibata, N. Oguma, and H. Harada, “Crack

Initiation from Micro Surface Holes in Bearings under Rolling Contact Fatigue," Fatigue and Fracture of Engineering Materials and Structures, Vol. 27, No 6, pp. 481–493, June 2004.

[31] P.M. Cann, M.N. Webster, J.P. Doner, and V. Wikstrom, "Grease Degradation in R0F Bearing Tests," Tribology Transactions, Vol. 50, No. 2, pp. 187–197, 2007.

[32] M. Naka, "Research and Development of Lubrication Greases by NSK," NSK Technical Journal Motion & Control, No.3, 1997.

[33] J. Zarei, "Induction Motors Bearing Fault Detection Using Pattern Recognition Techniques," Expert Systems with Applications, Vol. 39, pp. 68–73, 2012.

[34] B. Samanta, K.R. Al-Balushi, and S.A. Al-Araimi, "ANN and SVM with Genetic Algorithm for Bearing Fault Detection," Engineering Application of Artificial Intelligence, Vol. 16, pp. 657–665, 2003.

[35] K.C. Gryllias and I.A. Antoniadis, "A Support Vector Machine Approach Based on Physical Model Training for Rolling Element Bearing Fault Detection," Engineering Application of Artificial Intelligence, Vol. 25, pp. 326–344, 2012.

[36] P. Konar and P. Chattopadhyay, "Bearing Fault Detection of Induction Motor Using Wavelet and Support Vector Machines," Applied Soft Computing, Vol. 11, pp. 4203–4211, 2011.

[37] V. Sugumaran, G.R. Sabareesh, and K.I. Ramachandran, "Fault Diagnostics of Roller Bearing Using Kernel based Neighborhood Score Multi Class Support

Vector Machine," Expert Systems with Applications, Vol. 34, pp. 3090–3098, 2008.

[38] A. Rojas and A.K. Nandi, "Practical Scheme for Fast Detection and Classification of Rolling Element Bearing Faults Using Support Vector Machines," Mechanical Systems and Signal Processing, Vol. 20, pp. 1523–1536, 2006.

[39] A. Widodo, E.Y. Kim, J. Son, B. Yang, A.C.C. Tan, D. Gu, B. Choi, and J. Mathew, "Fault Diagnosis of Low Speed Bearing Based on Relevance Vector Machine and Support Vector Machine," Expert Systems with Applications, Vol. 36, pp. 7252–7261, 2009.

[40] C.T. Yiakopoulos, K.C. Gryllias, and I.A. Antoniadis "Rolling Element Bearing Fault Detection in Industrial Environments based on K-Means Clustering Approach," Expert Systems with Applications, Vol. 38, pp. 2888–2911, 2011.

[41] T. Boutros and M. Liang, "Detection and Diagnosis of Bearing and Cutting Tool Faults Using Hidden Markov Models," Mechanical Systems and Signal Processing, Vol. 25, pp. 2102–2124, 2011.

[42] V. Sugumaran and K.I. Ramacandran, "Automatic Rule Learning Using Decision Tree for Fuzzy Classifier in Fault Diagnosis of Roller Bearing," Mechanical Systems and Signal Processing, Vol. 21, pp. 2237–2247, 2007.

[43] P.D. McFadden and J.D. Smith, "Vibration Monitoring of Rolling Element Bearings by the High Frequency Resonance Technique – Review," Tribology International, Vol.17, Issue 1, pp. 3–10, February 1984.

[44] Y.T. Sheen, and C.K. Hung, “Constructing a Wavelet-based Envelope Function for Vibration Signal Analysis,” Mechanical Systems and Signal Processing, Vol. 18, No. 1, pp. 119–126, 2004.

[45] D.F. Shi, W.J. Wang, and L.S. Qu, “Defect Detection for Bearings Using Envelope Spectra of Wavelet Transform,” Journal of Vibration and Acoustics, Vol. 126, Issue 4, pp. 567–573, October 2004.

[46] J. Shiroishi, Y. Li, T. Kurfess, and S. Danyluk, “Bearing Condition Diagnostics via Vibration and Acoustic Emission Measurements,” Mechanical Systems and Signal Processing, Vol. 11, pp. 693–705, 1997.

[47] H. Qiu, J. Lee, J. Lin, and G. Yu, “Wavelet Filter-based Weak Signature Detection Method and its Application on Rolling Element Bearing Prognostics,” Journal of Sound and Vibration, Vol. 289, pp. 1066–1090, 2006.

[48] F. Immovilli, M. Cocconcelli, A. Bellini, and R. Rubini, “Detection of Generalized-Roughness Bearing Fault by Spectral-Kurtosis Energy of Vibration or Current Signals,” IEEE Transactions on Industrial Electronics, Vol. 56, No. 11, pp. 4710–4717, November 2009.

[49] M. Pecht, Prognostics and Health Management of Electronics, Wiley-Interscience, New York, pp. 47–68, 2008.

[50] Y. Li, T.R. Kurfess, and S.Y. Liang, “Stochastic Prognostics for Rolling Element Bearings,” Mechanical Systems and Signal Processing, Vol. 14, pp. 747–762, 2000.

[51] J. Qiu, C. Zhang, B. Seth, and S. Liang, “Damage Mechanics Approach for Bearing Lifetime Prognostics,” Mechanical Systems and Signal Processing,

Vol. 16, Issue 5, pp. 817–829, 2002.

[52] A. Beheshti and M. Khonsari, “On the Prediction of Fatigue Crack Initiation in Rolling/Sliding Contacts with Provision for Loading Sequence Effect,” Tribology International, Vol. 44, pp. 1620–1628, 2011.

[53] G.J. Kacprzynski, A. Sarlashkar, M.J. Roemer, A. Hess, and B. Hardman, “Predicting Remaining Life by Fusing the Physics of Failure Modeling with Diagnostics,” Journal of the Minerals, Metals and Materials Society, Vol. 56, pp. 29–35, 2004.

[54] C. Cempel, “Simple Condition Forecasting Techniques in Vibroacoustical Diagnostics,” Mechanical Systems and Signal Processing, Vol. 1, pp. 75–82, 1987.

[55] Y. Shao and K. Nezu, “Prognosis of Remaining Bearing Life Using Neural Networks,” Proceedings of the Institution of Mechanical Engineers, Part I: Journal of Systems and Control Engineering, pp. 217–230, 2000.

[56] P. Tse and D. Atherton, “Prediction of Machine Deterioration Using Vibration Based Fault Trends and Recurrent Neural Networks,” Transactions of the ASME: Journal of Vibration and Acoustics, Vol. 121, pp. 355–362, 1999.

[57] R.C.M. Yam, P.W. Tse, L. Li, and P. Tu, “Intelligent Predictive Decision Support System for CBM,” The International Journal of Advanced Manufacturing Technology, Vol. 17, pp. 383–391, 2001.

[58] H.T. Pham and B.S. Yang, “Estimation and Forecasting of Machine Health Condition Using ARMA/GARCH Model,” Mechanical Systems and Signal Processing, Vol. 24, pp. 546–558, 2010.

[59] N. Gebraeel, M. Lawley, R. Liu, and V. Parmeshwaran, "Residual Life Predictions from Vibration-based Degradation Signals: A Neural Network Approach," IEEE Transactions on Industrial Electronics, Vol. 51, pp. 694–700, 2004.

[60] R. Huang, L. Xi, X. Li, C. R. Liu, H. Qiu, and J. Lee, "Residual Life Predictions for Ball Bearings based on Self-organizing Map and Back Propagation Neural Network Methods," Mechanical Systems and Signal Processing, Vol. 21, pp. 193–207, 2007.

[61] M. Orchard and G. Vachtsevanos, "A Particle-filtering Approach for On-line Fault Diagnosis and Failure Prognosis," Transactions of the Institute of Measurement and Control, Vol. 31, pp. 221–246, 2009.

[62] C. Chen, B. Zhang, G. Vachtsevanos, and M. Orchard, "Machine Condition Prediction Based on Adaptive Neuro-Fuzzy and High-Order Particle Filtering," IEEE Transactions on Industrial Electronics, Vol. 58, pp. 4353–4364, 2011.

[63] B. Saha, K. Goebel, "Model Adaptation for Prognostics in a Particle Filtering Framework," International Journal of the PHM Society, Vol. 2, No. 1, Article No. 006, 2011.

[64] J. Sun, H. Zuo, W. Wang, and M. Pecht, "Application of a State Space Modeling Technique to System Prognostics Based on a Health Index for Condition-Based Maintenance," Mechanical Systems and Signal Processing, Vol. 28, pp. 585–596, 2012.

[65] R.R. Zhou, N. Serban, and N. Gebraeel, "Degradation Modeling Applied to Residual Lifetime Prediction Using Functional Data Analysis," The Annals of Applied Statistics, Vol. 5, No. 2B, pp. 1586–1610, 2011.

[66] ISO 10302-2: Acoustics—Measurement of Airborne Noise Emitted and Structure-borne Vibration Induced by Small Air-moving Devices—Part 2: Structure-borne Vibration Measurements, First Edition, International Organization for Standardization, Geneva, Switzerland, 2011.

[67] N. Judge, "Pick a Parameter… But Not Just Any Parameter," Manufacturing Engineering, Vol. 129, No. 4, October 2002.

[68] Veeco Instruments, Inc, AN505: Surface Measurement Parameters for Wyko Optical Profilers, Tucson, AZ, 2003.

[69] W. He, N. Williard, M. Osterman, and M. Pecht, "Prognostics of Lithium-ion Batteries Based on Dempster-Shafer Theory and the Bayesian Monte Carlo Method," Journal of Power Sources, Vol. 196, pp. 10314–10321, 2011.

[70] J. Sun, H. Zuo, W. Wang, and M. Pecht, "Application of a State Space Modeling Technique to System Prognostics Based on a Health Index for Condition-Based Maintenance," Mechanical Systems and Signal Processing, Vol. 28, pp. 585–596, 2012.

[71] M.H. Kalos, P.A. Whitlock, Monte Carlo methods. Volume I: Basics, Wiley, 1986.

[72] M. Aruampalam, S. Maskell, N. Gordon, and T. Clapp, "A Tutorial on Particle Filters for Online Nonlinear/Non-Gaussian Bayesian Tracking," IEEE Transactions on Signal Processing, Vol. 50, No. 2, pp. 174–188, 2002.

[73] F. Cadini, E. Zio, and D. Avram, “Monte Carlo-Based Filtering for Fatigue Crack Growth Estimation,” Probabilistic Engineering Mechanics, Vol. 24, pp. 367–373, 2009.

[74] A. Wald, “Sequential Tests of Statistical Hypotheses,” The Annals of Mathematical Statistics, Vol. 16, No. 2, pp. 117–196, 1945.

[75] ECMA-275: Measurement of Structure-borne Vibration Induced by Small Air Moving Devices (AMDs), Second Edition, ECMA International, Geneva, Switzerland, December 2002.

[76] IPC-9591: Performance Parameters (Mechanical, Electrical, Environmental and Quality/Reliability) for Air Moving Devices, First Edition, Institute for Interconnecting and Packaging Electronic Circuits (IPC), Bannockburn, IL, April 2006.